

Black hole shadows as new tests of general relativity

Alexander F. Zakharov

NRC «Kurchatov Institute», Moscow

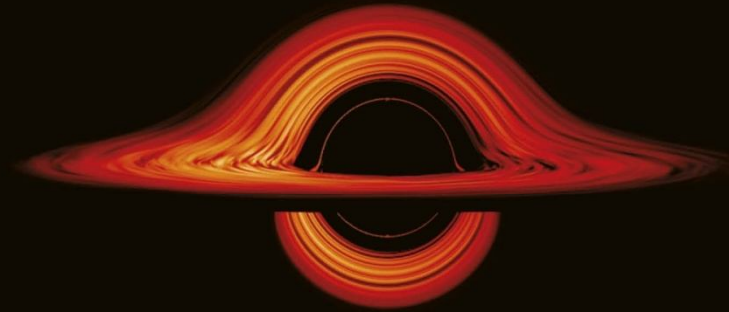
BLTP, JINR, Dubna

21st Lomonosov Conference on Elementary Particle Physics
MSU, Moscow, 29 August 2023

'A majestic story'
Financial Times



MICHIO
KAKU



THE GOD
EQUATION

The Quest for a
Theory of Everything

Our recent publications on the subject

AFZ, Phys. Part. Nucl. Lett. (2023)

AFZ, Universe (2022)

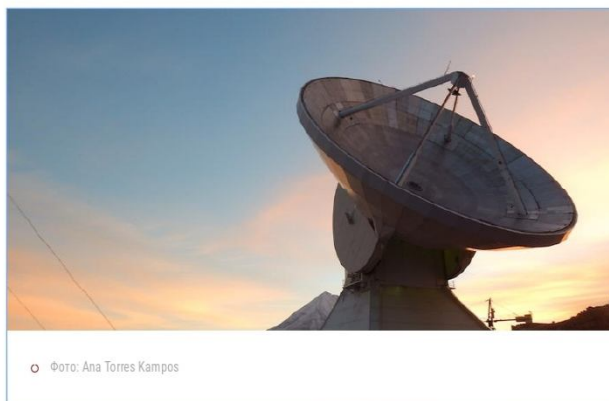
AFZ, Astron. Astrophys. Trans. (2022)

P. Jovanovic, D. Borka, V. Borka Jovanovic, AFZ, JCAP (2023)

AFZ, Phys. Part. Nucl. (2023)

Подтверждено предсказание ученого НИЦ "Курчатовский институт" о существовании "тени" в центре нашей Галактики

15.06.2022 ПРЕСС-ЦЕНТР НИЦ "КУРЧАТОВСКИЙ ИНСТИТУТ"



В 2005 году физик-теоретик **Александр Захаров** и его соавторы предложили с помощью наблюдений подтвердить присутствие сверхмассивной черной дыры в Центре нашей Галактики и проверить предсказания общей теории относительности в сильном гравитационном поле. А. Захаров и его итальянские коллеги предположили, что в случае наличия черной дыры в Галактическом центре (ГЦ) наблюдатели в направлении на ГЦ увидят тень размером порядка 52 микроарксекунд. Работа была опубликована в журнале [New Astronomy](#). 

"Понятие "черная дыра" для теоретика и наблюдателя отличается, – поясняет ведущий научный сотрудник лаборатории физики плазмы и астрофизики НИЦ "Курчатовский институт" Александр Захаров (в 2005 г. – сотрудник ИТЭФ). – Для теоретика черная дыра – это определенная метрика, описывающая пространство-время и являющаяся "вакуумным" решением уравнений Эйнштейна с определенными свойствами. А для наблюдателя – темное пятно или,

Outline of my talk

- Introduction
- Keck and GRAVITY (VLT) observations and corresponding constraints on GC models
- Schwarzschild precession discovery by GRAVITY and constraints on model parameters
- RAR or SMBH in GC
- Shadows at Sgr A* and M87*
- Conclusions

Black hole types

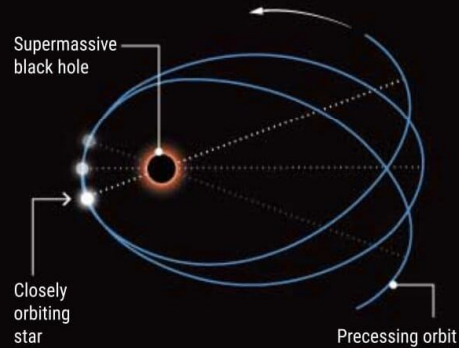
- Black holes with stellar masses $10 - 10^2 M_{\text{Sun}}$
- Massive black holes $10^2 - 10^5 M_{\text{Sun}}$
- Supermassive black holes $10^5 - 10^{10} M_{\text{Sun}}$
- Cosmological black holes $\gg 10^{10} M_{\text{Sun}}$

How to probe a black hole

Albert Einstein's theory of gravity, general relativity, predicts that the collapse of enough mass can leave a self-sustaining gravitational field so strong that, inside a distance called the event horizon, nothing can escape, not even light. But are black holes exactly the inscrutable things general relativity predicts? Observers may now have the tools to find out.

1. Trace the stars

Tracking the orbits of stars around the black hole in our Galaxy's center can reveal whether the black hole warps space and time exactly as general relativity predicts.



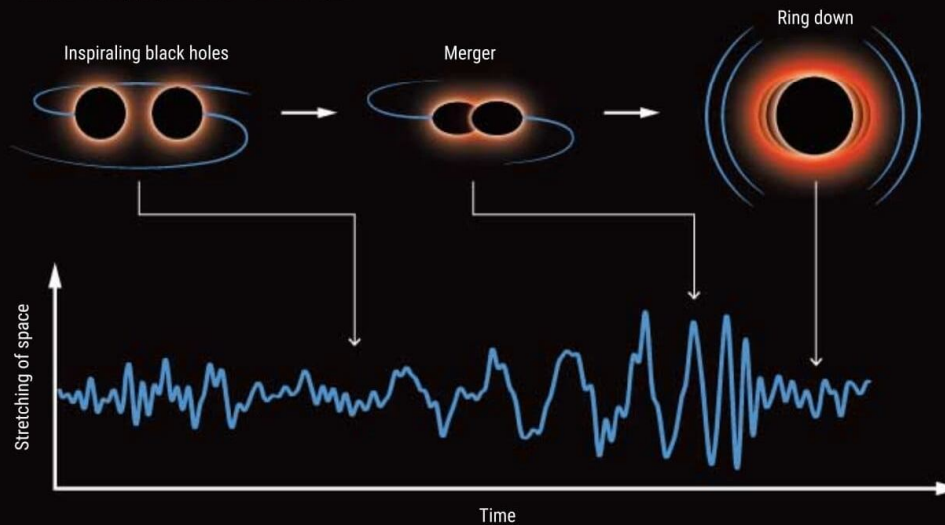
2. Take a picture

An image of a supermassive black hole holds clues to whether, as general relativity predicts, it has an event horizon rather than a surface, and mass and spin are its sole properties.



3. Catch the waves

When two small black holes spiral together, they radiate gravitational waves, which could reveal whether the supposed black holes are instead material objects. The final black hole reverberates at frequencies and overtones that provide another test of whether its only properties are mass and spin.



61 years since the Jablonna Conference (GR3) and 66 years since the Chapel Hill Conference (GR1)

Gen Relativ Gravit (2014) 46:1718
DOI 10.1007/s10714-014-1718-y

HISTORY

The Jablonna conference on gravitation: a continuing source of inspiration

Marek Demianski

Received: 21 January 2014 / Accepted: 11 March 2014 / Published online: 23 May 2014
© The Author(s) 2014. This article is published with open access at Springerlink.com

First of all I would like to welcome all of you at the main campus of the University of Warsaw—my University. Especially warmly I would like to welcome the youngest participants who for the first time participate in a big international conference. I do understand how you feel, I do understand your anxiety. Fifty one years ago I was able to observe the International Jablonna Conference on General Relativity and Gravitation, that later was classified as the GRG-3 conference. In June of 1962, I got my Master of Science degree in physics. My thesis advisor, Professor Leopold Infeld, was the Chairman of the Local Organizing Committee of the Jablonna conference. Professor Infeld asked me to help with such simple tasks as cleaning the blackboard, make sure that chalk was always available, but also—and this was really important—every morning to collect participants who were staying in hotels in Warsaw into a special coach and bring them in time to Jablonna, and in the evening bring them back to Warsaw. So that is how I ended up listening to all lectures and discussions and more. Now looking back from the perspective of half a century I think that the Jablonna Conference was the most important scientific conference that I attended so far.

The opening session of the Jablonna conference was held at the Staszica Palace in Warsaw, a short walk from where we are now. It is an easy recognizable building, in front of it is the famous monument of Copernicus (Fig. 1). The first talk was delivered by Professor J. L. Synge on “Relativistic interpretation and modification of Newtonian models”. On Fig. 2 is Professor J. Synge delivering his talk and, in the first row (from the left) Professors L. Infeld, V. Fock, J. Anderson, T. Newman, R. Penrose and B. Hoffman, and on the far right Dr. Róża Michalska-Trautman. After the first talk,



Fig. 1 The Staszica Palace in Warsaw



Fig. 2 Professor J. Synge delivering the opening lecture

followed by a short discussion, the session was adjourned and all participants were transferred to Jablonna.

Jablonna is a small town about 20 km from Warsaw. In XVIII century a famous Polish aristocratic family of Poniatowski built there a summer palace and two adjacent buildings with several rooms for their guests and servants. The Palace was surrounded

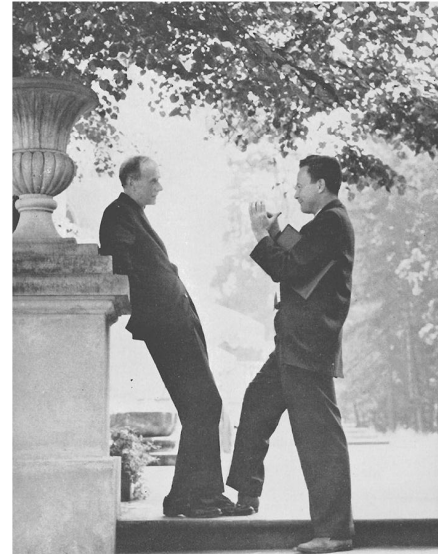
Leopold Infeld (20.08.1998 – 15.01.1968). He was one of the founders of JINR.



A. Einstein and L. Infeld in Princeton in 1930s



Fig. 6 Paul Dirac and Richard Feynman at Jablonna



the 2nd World War such a large group of physicists from the West and the East were able to meet. There were continuous discussions, usually in small groups between scientists coming from the West and the East. Also Germans from the DDR and the Bundes Republik were able to meet for the first time since the construction of the Berlin wall. It was a conference attended by many outstanding scientists. All leading physicists working at that time on general relativity and gravitation were present in Jablonna, including P. A. M. Dirac, R. Feynman, J. A. Wheeler, P. G. Bergmann, H. Bondi, S. Chandrasekhar, B. DeWitt, V. Ginzburg, D. Ivanenko, A. Lichnerowicz, C. Moller, L. Rosenfeld and J. Weber among others. One can say that Jablonna was a nesting place of Nobel Prize winners—Paul Dirac, Richard Feynman, Subrahmanyan Chandrasekhar, Vitali Ginzburg and also Peter Higgs were there. The main topics of discussions in Jablonna concentrated on general properties of gravitational radiation, quantization of gravity and exact solutions of the Einstein field equations. Only one talk given by Vitali Ginzburg was devoted to observational tests of general relativity (Figs. 6, 7, 8).

The most memorable lecture, in a dynamic showman style, was delivered by Richard Feynman. He presented his program of quantizing general relativity modeled on his very successful approach to quantum electrodynamics. Of course, he used Feynman diagrams. I am sure that Abhay Ashtekar will tell you more about it. After the conference I have listened to Feynman's talk many times trying to transcribe it from tapes. Fortunately John Stachel stayed in Warsaw for several months after the conference

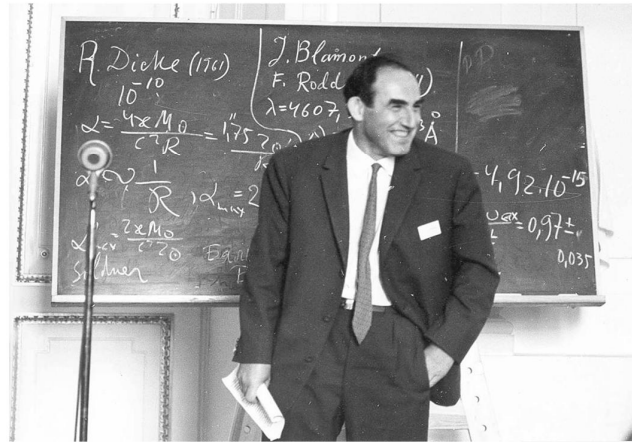


Fig. 7 Vitali Ginzburg delivering his lecture at the Jablonna conference

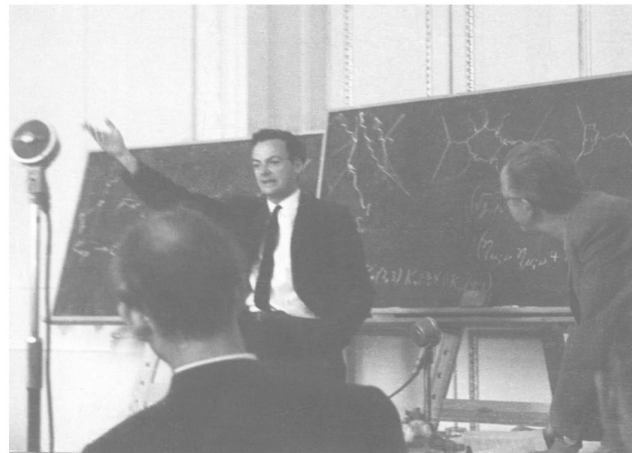


Fig. 8 Richard Feynman delivering his lecture at the Jablonna conference

“Incidentally, to give you some idea of the difference in order to calculate this diagram Fig. 4b the Young-Mills case took me about a day; to calculate the diagram in the case of gravitation I tried again and again and was never able to do it; and it was finally put on a computing machine—I don’t mean the arithmetic, I mean the algebra of all the terms coming in, just the algebra; I did the integrals myself later, but the algebra of the thing was done on a machine by John Matthews so I couldn’t done it by hand. In fact, I think it’s historically interesting that it’s the first problem in algebra that I know of that was done on a machine that has not been done by hand.” Just for

Great success of relativistic astrophysics

Three Nobel prizes in last five years (2017, 2019, 2020)

LIGO-Virgo: BBHs, BNS (kilonova) GW 170817;
GRAVITY, Keck and new tests of GR (gravitational
redshift for S2 near its periapsis passage)

The confirmation of relativistic precession for S2
(GRAVITY)

Shadow reconstructions in M87* and Sgr A*

ON A STATIONARY SYSTEM WITH SPHERICAL SYMMETRY
CONSISTING OF MANY GRAVITATING MASSES

BY ALBERT EINSTEIN
(Received May 10, 1939)

If one considers Schwarzschild's solution of the static gravitational field of spherical symmetry

$$(1) \quad ds^2 = -\left(1 + \frac{\mu}{2r}\right)^4 (dx_1^2 + dx_2^2 + dx_3^2) + \left(\frac{1 - \frac{\mu}{2r}}{1 + \frac{\mu}{2r}}\right)^2 dt^2$$

it is noted that

$$g_{44} = \left(\frac{1 - \frac{\mu}{2r}}{1 + \frac{\mu}{2r}}\right)^2$$

vanishes for $r = \mu/2$. This means that a clock kept at this place would go at the rate zero. Further it is easy to show that both light rays and material particles take an infinitely long time (measured in "coördinate time") in order to reach the point $r = \mu/2$ when originating from a point $r > \mu/2$. In this sense the sphere $r = \mu/2$ constitutes a place where the field is singular. (μ represents the gravitating mass.)

There arises the question whether it is possible to build up a field containing such singularities with the help of actual gravitating masses, or whether such regions with vanishing g_{44} do not exist in cases which have physical reality. Schwarzschild himself investigated the gravitational field which is produced by an incompressible liquid. He found that in this case, too, there appears a region with vanishing g_{44} if only, with given density of the liquid, the radius of the field-producing sphere is chosen large enough.

This argument, however, is not convincing; the concept of an incompressible liquid is not compatible with relativity theory as elastic waves would have to travel with infinite velocity. It would be necessary, therefore, to introduce a compressible liquid whose equation of state excludes the possibility of sound signals with a speed in excess of the velocity of light. But the treatment of any such problem would be quite involved; besides, the choice of such an equation of state would be arbitrary within wide limits, and one could not be sure that thereby no assumptions have been made which contain physical impossibilities.

One is thus led to ask whether matter cannot be introduced in such a way that questionable assumptions are excluded from the very beginning. In fact this can be done by choosing, as the field-producing mass, a great number of

The following table gives μ and $2r_0$ for $M = 1$ as functions of σ_0 (approximately):

σ_0	μ	$2r_0$
0.	1.	∞
.05	.988	19.76
.1	.948	9.48
.15	.97	6.56
.2	1.13	5.65
.23	1.32	5.63
.25	1.82	7.40
.26	2.63	10.1
.268	∞	∞

When the cluster is contracted from an infinite diameter its mass decreases at the most about 5%. This minimal mass will be reached when the diameter $2r_0$ is about 9. The diameter can be further reduced down to about 5.6, but only by adding enormous amounts of energy. It is not possible to compress the cluster any more while preserving the chosen mass distribution. A further addition of energy enlarges the diameter again. In this way the energy content, i.e. the gravitating mass of the cluster, can be increased arbitrarily without destroying the cluster. To each possible diameter there belong two clusters (when the number of particles is given) which differ with respect to the particle velocity.

Of course, these paradoxical results are not represented by anything in physical nature. Only that branch belonging to smaller σ_0 values contains the cases bearing some resemblance to real stars, and this branch only for diameter values between ∞ and $9M$.

The case of the cluster of the shell type, discussed earlier in this paper, behaves quite similarly to this one, despite the different mass distribution. The shell type cluster, however, does not contain a case with infinite μ , given a finite M .

The essential result of this investigation is a clear understanding as to why the "Schwarzschild singularities" do not exist in physical reality. Although the theory given here treats only clusters whose particles move along circular paths it does not seem to be subject to reasonable doubt that more general cases will have analogous results. The "Schwarzschild singularity" does not appear for the reason that matter cannot be concentrated arbitrarily. And this is due to the fact that otherwise the constituting particles would reach the velocity of light.

This investigation arose out of discussions the author conducted with Professor H. P. Robertson and with Drs. V. Bargmann and P. Bergmann on the mathematical and physical significance of the Schwarzschild singularity. The problem quite naturally leads to the question, answered by this paper in the negative, as to whether physical models are capable of exhibiting such a singularity.

Coevolution (Or Not) of Supermassive Black Holes and Host Galaxies

John Kormendy¹ and Luis C. Ho²

¹Department of Astronomy, University of Texas at Austin,
2515 Speedway C1400, Austin, TX 78712-1205; email: kormendy@astro.as.utexas.edu

²The Observatories of the Carnegie Institution for Science,
813 Santa Barbara Street, Pasadena, CA 91101; email: lho@obs.carnegiescience.edu

Abstract

Supermassive black holes (BHs) have been found in 87 galaxies by dynamical modeling of spatially resolved kinematics. The *Hubble Space Telescope* revolutionized BH research by advancing the subject from its proof-of-concept phase into quantitative studies of BH demographics. Most influential was the discovery of a tight correlation between BH mass M_\bullet and the velocity dispersion σ of the bulge component of the host galaxy. Together with similar correlations with bulge luminosity and mass, this led to the widespread belief that BHs and bulges coevolve by regulating each other's growth. Conclusions based on one set of correlations from $M_\bullet \sim 10^{9.5} M_\odot$ in brightest cluster ellipticals to $M_\bullet \sim 10^6 M_\odot$ in the smallest galaxies dominated BH work for more than a decade.

New results are now replacing this simple story with a richer and more plausible picture in which BHs correlate differently with different galaxy components. A reasonable aim is to use this progress to refine our understanding of BH - galaxy coevolution. BHs with masses of $10^5 - 10^6 M_\odot$ are found in many bulgeless galaxies. Therefore, classical (elliptical-galaxy-like) bulges are not necessary for BH formation. On the other hand, while they live in galaxy disks, BHs do not correlate with galaxy disks. Also, any M_\bullet correlations with the properties of disk-grown pseudobulges and dark matter halos are weak enough to imply no close coevolution.

The above and other correlations of host galaxy parameters with each other and with M_\bullet suggest that there are four regimes of BH feedback. (1) Local, secular, episodic, and stochastic feeding of small BHs in largely bulgeless galaxies involves too little energy to result in coevolution. (2) Global feeding in major, wet galaxy mergers rapidly grows giant BHs in short-duration, quasar-like events whose energy feedback does affect galaxy evolution. The resulting hosts are classical bulges and coreless-rotating-disky ellipticals. (3) After these AGN phases and at the highest galaxy masses, maintenance-mode BH feedback into X-ray-emitting gas has the primarily negative effect of helping to keep baryons locked up in hot gas and thereby keeping galaxy formation from going to completion. This happens in giant, core-nonrotating-boxy ellipticals. Their properties, including their tight correlations between M_\bullet and core parameters, support the conclusion that core ellipticals form by dissipationless major mergers. They inherit coevolution effects from smaller progenitor galaxies. Also, (4) independent of any feedback physics, in BH growth modes (2) and (3), the averaging that results from successive mergers plays a major role in decreasing the scatter in M_\bullet correlations from the large values observed in bulgeless and pseudobulge galaxies to the small values observed in giant elliptical galaxies.

Table 1 Mass measurements of supermassive black holes in our Galaxy, M31, and M32

Galaxy	D (Mpc)	σ_e (km s ⁻¹)	M_\bullet ($M_{\text{low}}, M_{\text{high}}$) (M_\odot)	r_{infl} (arcsec)	σ_* (arcsec)	r_{infl}/σ_*	Reference
(1)	(2)	(3)	(4)	(5)	(6)	(7)	(8)
Galaxy			4.41(3.98–4.84) e6		0.0146	2868.	Meyer et al. 2012
Galaxy			4.2 (3.9 – 4.6) e6		0.0139	3013.	Yelda et al. 2011
Galaxy	0.00828	105	4.30(3.94–4.66) e6	41.9	0.0146	2868.	Genzel, Eisenhauer & Gillessen 2010
Galaxy	0.00828	105	4.30(3.94–4.66) e6	41.9	0.0146	2868.	Gillessen et al. 2009a
Galaxy			4.09(3.74–4.43) e6		0.0148	2829.	Gillessen et al. 2009b
Galaxy			4.25(3.44–4.79) e6		0.0139	3013.	Ghez et al. 2008
Galaxy			3.80(3.60–4.00) e6		0.0056	7478.	Ghez et al. 2005
Galaxy			3.7 (3.3 – 4.1) e6		0.0075	5583.	Ghez et al. 2003
Galaxy			3.8 (2.3 – 5.4) e6		0.0155	2702.	Schödel et al. 2002
Galaxy			2.1 (1.3 – 2.8) e6		0.113	371.	Chakrabarty & Saha 2001
Galaxy			3.1 (2.6 – 3.6) e6		0.26	161.	Genzel et al. 2000
Galaxy			2.7 (2.5 – 2.9) e6		0.39	107.	Ghez et al. 1998
Galaxy			2.70(2.31–3.09) e6		0.39	107.	Genzel et al. 1997
Galaxy			2.55(2.12–2.95) e6		0.39	107.	Eckart & Genzel 1997
Galaxy			2.8 (2.5 – 3.1) e6		2.4	17.4	Genzel et al. 1996
Galaxy			2.0 (0.9 – 2.9) e6		4.9	8.5	Haller et al. 1996
Galaxy			2.9 (2.0 – 3.9) e6		3.4	12.3	Krabbe et al. 1995
Galaxy			2. e6		5	8.4	Evans & de Zeeuw 1994
Galaxy			3. e6		5	8.4	Kent 1992
Galaxy			5.4 (3.9 – 6.8) e6		15	2.8	Sellgren et al. 1990
M31	0.774	169	1.4 (1.1–2.3) e8	5.75	0.053	109.	Bender et al. 2005
M31			1.0 e8		0.297	19.4	Peiris & Tremaine 2003
M31			6.1 (3.6–8.7) e7		0.052	111.	Bacon et al. 2001
M31			3.3 (1.5–4.5) e7		0.297	19.4	Kormendy & Bender 1999
M31			6.0 (5.8–6.2) e7		0.297	19.4	Magorrian et al. 1998
M31			9.5 (7 – 10) e7		0.42	13.7	Emsellem & Combes 1997
M31			7.5 e7		0.56	10.3	Tremaine 1995
M31			8.0 e7		0.42	13.7	Bacon et al. 1994
M31			5 (4.5–5.6) e7		0.59	9.7	Richstone, Bower & Dressler 1990
M31			3.8 (1.1– 11) e7		0.56	10.3	Kormendy 1988a
M31			5.6 (3.4–7.8) e7		0.59	9.7	Dressler & Richstone 1988
M32	0.805	77	2.45(1.4–3.5) e6	0.46	0.052	8.76	van den Bosch & de Zeeuw 2010
M32			2.9 (2.7–3.1) e6		0.052	8.76	Verolme et al. 2002
M32			3.5 (2.3–4.6) e6		0.052	8.76	Joseph et al. 2001
M32			2.4 (2.2–2.6) e6		0.23	1.98	Magorrian et al. 1998
M32			3.9 (3.1–4.7) e6		0.050	9.11	van der Marel et al. 1998a
M32			3.9 (3.3–4.5) e6		0.050	9.11	van der Marel et al. 1997a, 1997b
M32			3.2 (2.6–3.7) e6		0.23	1.98	Bender, Kormendy & Dehnen 1996
M32			2.1 (1.8–2.3) e6		0.34	1.34	Dehnen 1995
M32			2.1 e6		0.34	1.34	Qian et al. 1995
M32			2.1 (1.7–2.4) e6		0.34	1.34	van der Marel et al. 1994a
M32			2.2 (0.8–3.5) e6		0.59	0.77	Richstone, Bower & Dressler 1990
M32			9.3 e6		0.59	0.77	Dressler & Richstone 1988
M32			7.5 (3.5–11.5) e6		0.76	0.60	Tonry 1987
M32			5.8 e6		1.49	0.31	Tonry 1984

Lines based on HST spectroscopy are in red. Column 2 is the assumed distance. Column 3 is the stellar velocity dispersion inside the “effective radius” that encompasses half of the light of the bulge. Column 4 is the measured BH mass with the one-sigma range that includes 68% of the probability in parentheses. Only the top four M_\bullet values for the Galaxy include distance uncertainties in the error bars. Column 5 is the radius of the sphere of influence of the BH; the line that lists r_{infl} contains the adopted M_\bullet . Column 6 is the effective resolution of the spectroscopy, estimated as in Kormendy (2004). It is a radius that measures the blurring effects of the telescope point-spread function or “PSF,” the slit width or aperture size, and the pixel size. The contribution of the telescope is estimated by the dispersion σ_{tel} of a Gaussian fitted to the core of the average radial brightness profile of the PSF. In particular, the HST PSF has $\sigma_{\text{tel}} \approx 0.036$ from a single-Gaussian fit to the PSF model in van der Marel, de Zeeuw & Riv (1997a)

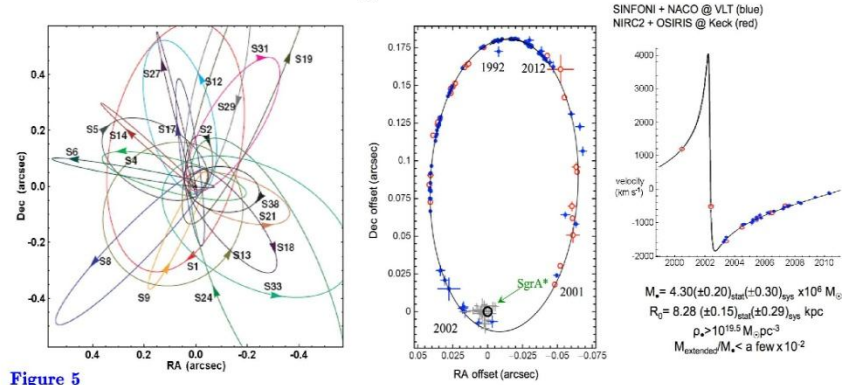


Figure 5

(left) Orbits of individual stars near the Galactic center. (right) Orbit of star S2 around the BH and associated radio source Sgr A* based on observations of its position from 1992 to 2012. Results from the Ghez group using the Keck telescope and from the Genzel group using the European Very Large Telescope (VLT) are combined. This figure is updated from Genzel, Eisenhauer & Gillessen (2010) and is kindly provided by Reinhard Genzel.

These results establish the existence and mass of the central dark object beyond any reasonable doubt. They also eliminate astrophysical plausible alternatives to a BH. These include brown dwarfs and stellar remnants (e. g., Maoz 1995, 1998; Genzel et al. 1997, 2000; Ghez et al. 1998, 2005) and even fermion balls (Ghez et al. 2005; GEG10). Bosen balls (Torres et al. 2000; Schunck & Mielke 2003; Liebling & Palenzuela 2012) are harder to exclude; they are highly relativistic, they do not have hard surfaces, and they are consistent with dynamical mass and size constraints. But a boson ball is like the proverbial elephant in a tree: it is OK where it is, but how did it ever get there? GEG10 argue that boson balls are inconsistent with astrophysical constraints based on AGN radiation. Also, the Soltan (1982) argument implies that at least most of the central dark mass observed in galaxies grew by accretion in AGN phases, and this quickly makes highly relativistic objects collapse into BHs. Finally (Fabian 2013), X-ray AGN observations imply that we see, in some objects, material interior to the innermost stable circular orbit of a non-rotating BH; this implies that these BHs are rotating rapidly and excludes boson balls as alternatives to all central dark objects. Arguments against the most plausible BH alternatives – failed stars and dead stars – are also made for other galaxies in Maoz (1995, 1998) and in Bender et al. (2005). Exotica such as sterile neutrinos or dark matter WIMPs could still have detectable (small) effects, but we conclude that they no longer threaten the conclusion that we are detecting supermassive black holes.

KR95 was titled “Inward Bound – The Search for Supermassive Black Holes in Galactic Nuclei.” HST has taken us essentially one order of magnitude inward in radius. A few other telescopes take us closer. But mostly, we are still working at 10^4 to 10^5 Schwarzschild radii. In our Galaxy, we have observed individual stars in to ~ 500 Schwarzschild radii. Only the velocity profiles of relativistically broadened Fe K α lines (e. g., Tanaka et al. 1995; Fabian 2013) probe radii that are comparable to the Schwarzschild radius. So we are still inward bound. Joining up our measurements made at thousands of r_S with those probed by Fe K α emission requires that we robustly integrate into our story the rich and complicated details of AGN physics; that is, the narrow- and broad-emission-line regions. That journey still has far to go.

Vitaly L. Ginzburg

The Physics of a Lifetime

Reflections on the Problems
and Personalities of 20th Century Physics



Springer

What Problems of Physics and Astrophysics Seem Now to Be Especially Important and Interesting (Thirty Years Later, Already on the Verge of the 21st Century)?¹

1. Introduction

The rate of development of science nowadays is striking. Great changes in physics, astronomy, biology, and many other fields of science have come about within a period of not more than one to two generations. Readers may see it even in the example of their own families. My father, for instance, was born in 1863 and was a younger contemporary of Maxwell (1831–1879). I myself was already 16 when the neutron and positron were discovered in 1932. Before that only the electron, proton, and photon were known. It is somehow not easy to realize that the electron, X-rays, and radioactivity were discovered only about a hundred years ago, and quantum theory was born in 1900. At the same time, one hundred years is such a short period, not only compared with the approximately 3 billion years since life appeared on the Earth, but also compared with the age of modern man (*Homo sapiens*), which amounts to nearly 50 thousand years! It is also useful to remember that the first great physicists – Aristotle (384–322 B.C.) and Archimedes (about 287–212 B.C.) are separated from us by more than two thousand years.

But the further progress of science was comparatively slow; in this, religious dogmatism played not the least part. Since the time of Galileo Galilei (1564–1642) and Kepler (1571–1630) the development of physics has been increasingly rapid. But, incidentally, even Kepler was of the opinion that there exists a sphere of motionless stars which “consists of ice or a crystal”. The fight of Galileo for the acknowledgment of heliocentric concepts, for which he was convicted by the Inquisition in 1633, is generally known. What a path has been traveled since then in only 300–400 years! The result is contemporary science. It has already freed itself from religious chains, and the church today at least does not deny the role of science [3]. True, pseudoscientific tendencies and the propagation of pseudoscience (especially astrology) do go on, in particular, in Russia. But it is only the triumph of totalitarianism (bolshevism–communism or fascism) that can radically obstruct the progress

¹ As mentioned in the Preface to the English translation of this book, the present paper, published in the journal *Physics–Uspekhi* **42**, 353, 1999, is a direct continuation or, more precisely, a development of the previous paper that opened the book. Some points are added here to the journal version, in particular, some references.

12. Rasers, grasers, superhigh-power lasers.
13. Superheavy elements. Exotic nuclei.
14. The mass spectrum. Quarks and gluons. Quantum chromodynamics. The quark-gluon plasma.
15. The unified theory of the weak and electromagnetic interactions. W^\pm and Z^0 bosons. Leptons.
16. The standard model. Grand unification. Superunification. Proton decay. Neutrino mass. Magnetic monopoles.
17. The fundamental length. Particle interaction at high and superhigh energies. Colliders.
18. Nonconservation of CP invariance.
19. Nonlinear phenomena in vacuum and in superstrong magnetic fields. Phase transitions in vacuum.
20. Strings. M-theory.
21. Experimental verification of the general theory of relativity.
22. Gravitational waves and their detection.
23. The cosmological problem. Inflation. The Λ term. The relationship between cosmology and high-energy physics.
24. Neutron stars and pulsars. Supernova stars.
25. Black holes. Cosmic strings (?).
26. Quasars and galactic nuclei. Formation of galaxies.
27. The problem of dark matter (hidden mass) and its detection.
28. The origin of ultrahigh-energy cosmic rays.
29. Gamma bursts. Hypernovae.
30. Neutrino physics and astronomy. Neutrino oscillations.

The singling out of 30 particular problems (more precisely, items in the 'list') is of course in a sense subjective. Moreover, some of them might be divided. In [1] there were 17 problems, in [2] there were already 23. In [7] 24 problems were listed. In the letters that came to *Physics Today* in respect of this note [7], the opinion [8] was expressed that the list should also have included star formation, atomic and molecular physics (true, I am unaware of what exactly was meant), and the question of exceedingly accurate measurements. I had to get acquainted with other suggestions that the list should be extended. Some of them have been taken into consideration, but others (for example, those concerning quantum computers, the 'optics' of atomic beams, and semiconductor devices) I had to ignore.

Any 'list' is undoubtedly not a dogma; some things can be discarded and some things added, depending on the preferences of lecturers and of authors of papers. More interesting is the question of the evolution of the list with time as it reflects the process of the development of physics. In the 'list' of 1970–1971 [1], quarks were given only three lines in the enumeration of the attempts to explain the mass spectrum. This did not testify to my perspicacity, which was admitted in [2]. However, at that time (in 1970) quarks were only five or six years old (I mean the age of the corresponding hypothesis), and the fate

Connection of GC puzzle and the Ginzburg's problems

25. Black holes. Cosmic strings.

26. Quasars and galactic nuclei. Formation of galaxies.

27. The problem of dark matter (hidden mass) and its detection.

The Ginzburg's review played a very important role for researchers to choose a problem for investigations.

**Shadow reconstructions for M87*
and Sgr A* are based on three
pillars: Synchrotron radiation,
VLBI concept, GR in a strong
gravitational field**

Synchrotron radiation (George A. Schott)



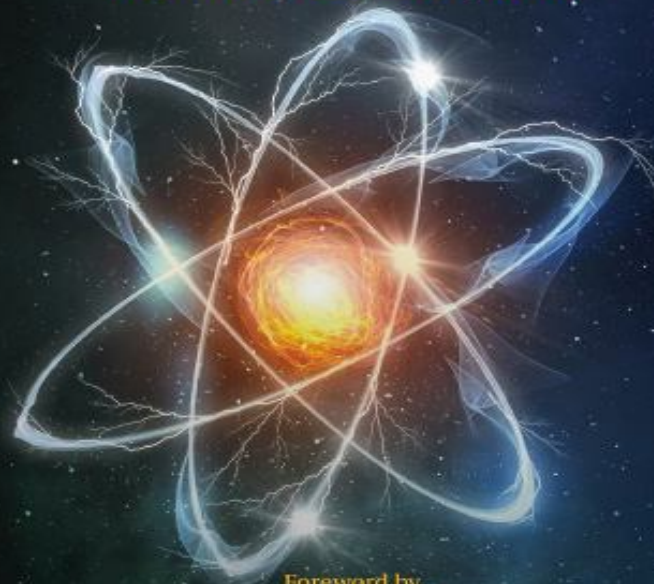
G. A. Schott

Forthcoming

THE
PLANETARY ATOM

A FICTIONAL ACCOUNT OF GEORGE ADOLPHUS SCHOTT
THE FORGOTTEN PHYSICIST

Jean-Patrick Connerade



Foreword by
Roald Hoffmann, Nobel Laureate in Chemistry

 World Scientific

ELECTROMAGNETIC RADIATION

AND THE MECHANICAL REACTIONS
ARISING FROM IT

BEING AN ADAMS PRIZE ESSAY IN THE
UNIVERSITY OF CAMBRIDGE

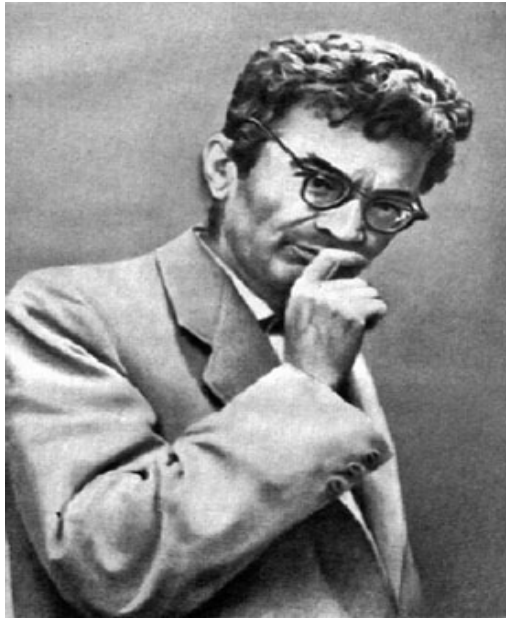
by

G. A. SCHOTT, B.A., D.Sc.

Professor of Applied Mathematics in the University College of Wales, Aberystwyth
Formerly Scholar of Trinity College, Cambridge

Cambridge :
at the University Press

1912



I. Pomeranchuk, The maximum energy that primary cosmic ray electrons can have on the Earth's surface due to radiation in the Earth's magnetic field, J. Phys. USSR, 2, 356 (1940)

D. Ivanenko and I. Pomeranchuk, On the Maximal Energy Attainable in a Betatron, Phys. Rev. 65, 343 (1944)

L.A. Artsimovich and I. Pomeranchuk, The maximum energy that primary cosmic ray electrons can have on the Earth's surface due to radiation in the Earth's magnetic field, J. Phys. USSR, 2, 267 (1945)

Elder, F. R., Gurewitsch, A. M., Langmuir, R. V., & Pollock, H. C. Radiation from Electrons in a Synchrotron. Physical Review, 71(11), 829 (1947)

In 1950 D. Ivanenko, A. A. Sokolov and I. Pomeranchuk were awarded the State prize of the second grade for works on synchrotron radiation, presented in book "Classical Field Theory"

Professor Arsenij Alexandrovich Sokolov and professor
Dmitrij Dmitrievich Ivanenko



Academician Lev Andreevich Artsimovich (the founder of the Atomic physics chair at Physical department of MSU, Academician secretary of the General Physics and Astronomy division of the Soviet Academy of Sciences, the chairman of the National committee of physicists)



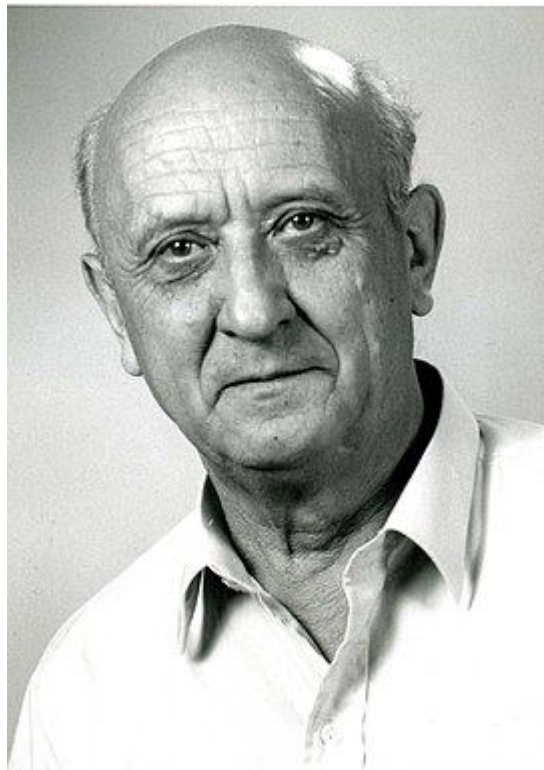
Synchrotron radiation plays a key role in many astrophysical objects (including BH's) . In 1946 they predicted emission in radio band from solar corona. In May 1947 they participated in Brazil expedition



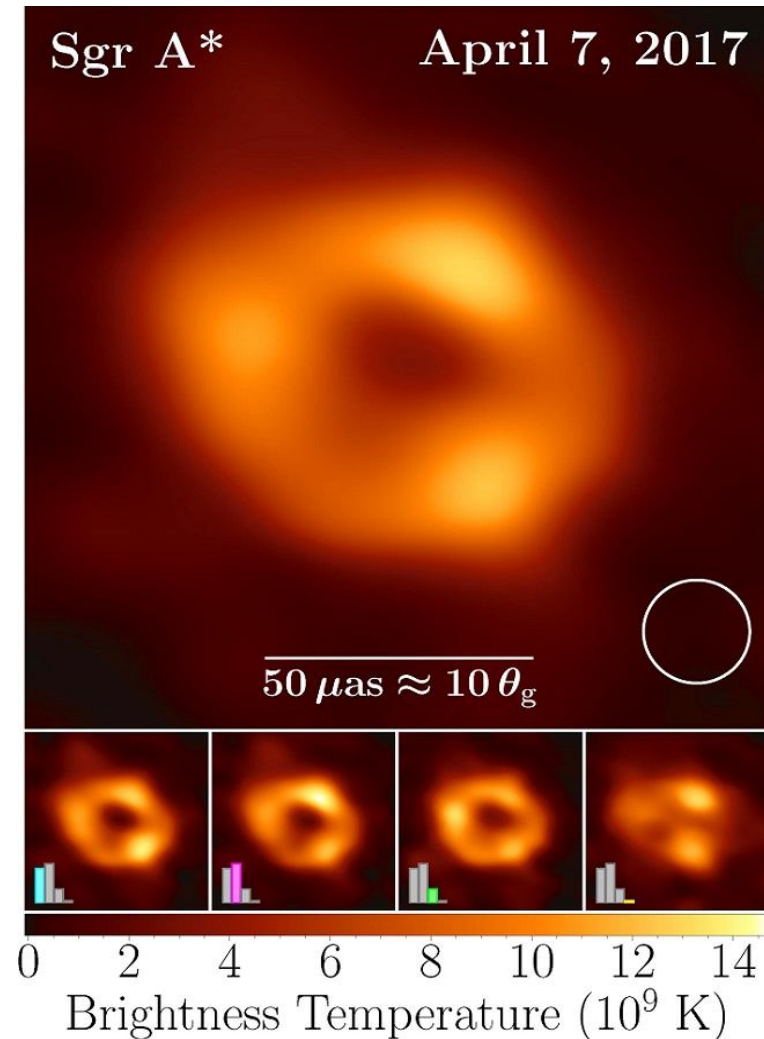
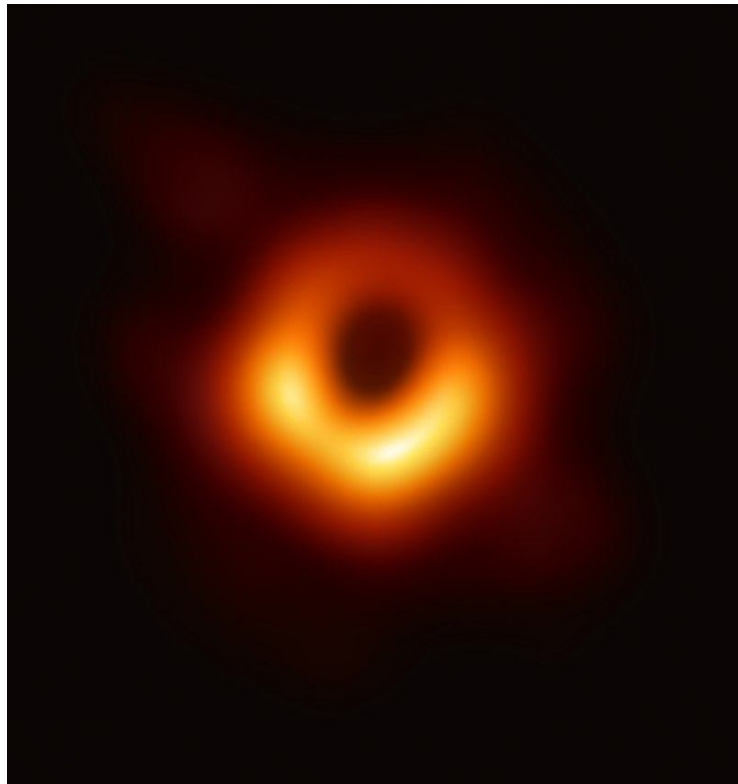
The Soviet expedition in Brazil for solar eclipse observations in 20 May 1947 where S. E. Khaikin and B. M. Chikhachev discovered radio emission from solar corona during the solar eclipse aboard the “Griboedov” ship



The idea of VLBI observation was introduced by L. I. Matveenko (1929—2019) in 1960s and it was realized in Soviet – US joint radio observations in 1970s. Matveenko proposed also a project of a ground – space interferometer. This idea was realized later by Japanese (HALCA, VSOP, 1997) and Russian Astronomers (Radioastron, 2011) .



EHT shadow reconstruction for M87* and Sgr A* observed in April 2017



<https://www.gazeta.ru/science/news/2022/06/15/17937578.shtml>

- 15 июня 2022, 16:03
- **Сбылось предсказание российского ученого о загадочной тени**
- [Борис Ганьжин](#)
-
- Первое изображение сверхмассивной черной дыры в центре Млечного Пути, о получении которого в мае 2022 года [сообщила](#) коллаборация Телескопа горизонта событий Event Horizon Telescope, послужило подтверждением предсказания ведущего научного сотрудника лаборатории физики плазмы и астрофизики ККТЭФ НИЦ «Курчатовский институт» Александра Захарова и его итальянских коллег, сделанного в 2005 году. Об этом «Газете.Ru» сообщили в НИЦ «Курчатовский институт».

**For about 20 years we declared black
holes (for theorists) are dark spots
(shadows) for observers**



Measuring the black hole parameters in the galactic center with RADIOASTRON

A.F. Zakharov^{a,b,c,*}, A.A. Nucita^d, F. DePaolis^d, G. Ingresso^d

^a *Institute of Theoretical and Experimental Physics, 25, B. Chermushkinskaya st., Moscow 117259, Russia*

^b *Space Research Centre of Lebedev Physics Institute, Moscow, Russia*

^c *Joint Institute for Nuclear Research, Dubna, Russia*

^d *Dipartimento di Fisica, Università di Lecce and INFN, Sezione di Lecce, Italy*

Received 19 January 2005; accepted 21 February 2005

Available online 23 March 2005

Communicated by F. Melchiorri

Abstract

Recently, Holz and Wheeler (2002) [ApJ 578, 330] considered a very attracting possibility to detect retro-MACHOs, i.e., retro-images of the Sun by a Schwarzschild black hole. In this paper, we discuss glories (mirages) formed near rapidly rotating Kerr black hole horizons and propose a procedure to measure masses and rotation parameters analyzing these forms of mirages. In some sense that is a manifestation of gravitational lens effect in the strong gravitational field near black hole horizon and a generalization of the retro-gravitational lens phenomenon. We analyze the case of a Kerr black hole rotating at arbitrary speed for some selected positions of a distant observer with respect to the equatorial plane of a Kerr black hole. Some time ago Falcke, Melia, Agol (2000) [ApJ 528, L13S] suggested to search shadows at the Galactic Center. In this paper, we present the boundaries for shadows. We also propose to use future radio interferometer RADIOASTRON facilities to measure shapes of mirages (glories) and to evaluate the black hole spin as a function of the position angle of a distant observer.

© 2005 Elsevier B.V. All rights reserved.

PACS: 97.60.L; 04.70; 95.30.S; 04.20; 98.62.S

Keywords: Black hole physics; Gravitational lenses; Microlensing

1. Introduction

Recently Holz and Wheeler (2002) have suggested that a Schwarzschild black hole may form retro-images (called retro-MACHOs) if it is illuminated by the Sun. We analyze a rapidly rotating

* Corresponding author. Tel.: +7 095 1299759; fax: +7 095 8839601.

E-mail address: zakharov@itep.ru (A.F. Zakharov).

Our proposal

In 2004-2005 we proposed a way to test GR predictions with Radioastron:

Since angular resolution of Radioastron at 1.3 cm is around 8 μ as and the size of darkness (shadow) could help us to evaluate a charge, while shape could help us to evaluate a spin (good!)

The shortest wavelength is 1.3 cm (it is too long to detect shadow) (not good for Radioastron!)

So, we propose to test GR predictions about shape and size of BH images with observations. Astronomy is dealing with images. Therefore, establishing the correspondence of theoretical image and reconstructed image using observational data is an aim for further observations.

AFZ et al., NA (2005): “In our old paper

<https://ui.adsabs.harvard.edu/.../2005NewA...10.../abstract>

we wrote at the end "In spite of the difficulties of measuring the shapes of images near black holes is so attractive challenge to look at the “faces” of black holes because namely the mirages outline the “faces” and correspond to fully general relativistic description of a region near black hole horizon without any assumption about a specific model for astrophysical processes around black holes (of course we assume that there are sources illuminating black hole surroundings). No doubt that the rapid growth of observational facilities will give a chance to measure the mirage shapes using not only RADIOASTRON facilities but using also other instruments and spectral bands (for example, X-ray interferometer MAXIM (White, 2000; Cash et al., 2000) or sub-mm VLBI array (Miyoshi, 2004)). Astro Space Centre of Lebedev Physics Institute proposed except the RADIOASTRON mission and developed also space based interferometers (Millimetron and Sub-millimetron) for future observations in mm and sub-mm bands. These instruments could be used for the determination of shadow shapes."

Types of unbound geodesics in the Kerr metric

A. F. Zakharov

Institute of Theoretical and Experimental Physics, Academy of Sciences of the USSR, Moscow

(Submitted 4 December 1985)

Zh. Eksp. Teor. Fiz. **91**, 3-6 (July 1986)

Sets of constants of motion of a particle that correspond to different types of r -motion are considered. The topology of these sets is determined and a number of constants characterizing these sets are found.

INTRODUCTION

An important problem in the study of unbound motion of particles in the Kerr metric is the description of the set of constants of motion for which a particle traveling from infinity goes below the horizon of a black hole. We shall give a qualitative description of this set and also of the set of constants of motion for which the particle asymptotically approaches a sphere placed around the black hole, and the sets of constants of motion for which the particle departs to infinity. The solution of this problem is important in connection with the accretion of noninteracting particles on a rotating black hole.

It is well-known that Kepler orbits are characterized by two constants (E and L), since we can identify orbits that can transform into one another by rotations through the Euler angles. Hence, orbits in the Schwarzschild metric are also characterized by two constants. It turns out that a change in the radial coordinate in the Kerr metric is determined by only three constants in the case of moving particles (because the particle mass characterizes the connection between the affine parameter and the proper time of the particle), and two constants in the case of the motion of photons (because of the photon energy characterizes the set of different affine parameters in the equation for the change in the r coordinate.)

1. BASIC NOTATION

The equation of motion for the radial variable in the Kerr metric is¹

$$R(r) = r^4 + (a^2 - \xi^2 - \eta)r^2 + 2M[\eta + (\xi - a)^2]r - a^2\eta \quad (\text{Photons}), \quad (1)$$

$$R(r) = r^4 + (a^2 - \xi^2 - \eta)r^2 + 2M[\eta + (\xi - a)^2]r - a^2\eta - r^2\Delta/E \quad (\text{Particles}),$$

where

$$\rho^2 = r^2 + a^2 \cos^2 \theta, \quad \Delta = r^2 - 2Mr + a^2, \quad a = S/M. \quad (2)$$

The constants S and M refer to the black hole, namely, S is the angular momentum and M the mass of the black hole. The constants E , ξ , and η refer to the particle, namely, E is its energy at infinity, $\xi = L_z/E$ (L_z is the angular momentum of the particle about the axis of rotation of the black hole), and $\eta = Q/E^2$ (Q is given by

$$Q = p_\theta^2 + \cos^2 \theta [a^2 (\mu^2 - E^2) + \sin^2 \theta L_z^2],$$

and μ is the mass of the particle). It is readily verified that

the radial motion of the particle depends on the following constants:

$$\hat{a} = a/M, \quad \hat{E} = E/\mu, \quad \hat{\xi} = \xi/M, \quad \hat{\eta} = \eta/M^2.$$

The radial motion of photons does not depend on the constant \hat{E} . Instead of the coordinate r , we now introduce $\hat{r} = r/M$. (The symbol \wedge will be omitted henceforth.) Thus, the character of motion in the r -coordinate for given value of \hat{a} is determined by the three constants \hat{E} , $\hat{\xi}$, $\hat{\eta}$ in the case of a moving particle, and by the two constants $\hat{\xi}$ and $\hat{\eta}$ in the case of photons.

Depending on the multiplicities of the roots of the polynomial $R(r)$ (for $r \gg r_g$), we can have three types of motion in the r -coordinate,² namely:

(1) the polynomial $R(r)$ has no roots (for $r \gg r_g$). The particle then falls into the black hole;

(2) the polynomial $R(r)$ has roots and $r_{\max} > r_g$ (r_{\max} is the maximum root); for $(\partial R / \partial r)(r_{\max}) \neq 0$ we then have, $(\partial R / \partial r)(r_{\max}) > 0$, and the particle departs to infinity after approaching the black hole;

(3) the polynomial $R(r)$ has a root and $R(r_{\max}) = (\partial R / \partial r)(r_{\max}) = 0$; the particle now takes an infinite proper time to approach the sphere of radius r_{\max} .

2. DESCRIPTION OF THE SET OF CONSTANTS CORRESPONDING TO DIFFERENT TYPES OF MOTION

We shall now examine the sets of constants of motion E , ξ , and η corresponding to different types of particles motion for a given black-hole rotation parameter $a = \text{const}$. Let us cut the space E, ξ, η with the plane $E = \text{const} > 1$ and describe in this slice the set of constants corresponding to different types of motion. It then turns out that the boundary of the set of constants corresponding to the second type of motion for $\eta > 0$ is the set of constants for which the motion belongs to the third type. We shall look upon this set as the graph of the function $\eta = \eta(\xi)$. We note that the set of these constants as functions $\xi(r)$ and $\eta(r)$ was examined by Chandrasekhar¹. Let us describe some of the properties of the function $\eta(\xi)$. If the motion of the particle is of the third type, we have

$$R(r) = 0, \quad (\partial R / \partial r)(r) = 0 \quad (3)$$

for $\eta > 0, r \gg r_g$.

Thus, to obtain the function $\eta(\xi)$, we must eliminate r from (3). Assuming that (3) provides an implicit specification of $r(\xi)$ and $\eta(\xi)$, we find that

$$d\eta/d\xi(-\Delta) = 2\xi^2 - 4(\xi - a)r, \quad (4)$$

$$d\eta/d\xi(-2r+2) + (d/d\xi)(\partial^2 R / \partial r^2) = 4\xi r - 4(\xi - a)$$

for $r > r_s, \eta > 0$. We note that, for $\Delta > 0$ and $\partial^2 R / \partial r^2 \neq 0$, the implicit function theorem shows that $r(\xi)$ and $\eta(\xi)$ are single-valued functions. Analysis similar to that given in Ref. 3 then shows that, when $a \neq 1$ or $\xi \neq 2$, we have $\partial^2 R / \partial r^2 > 0$. When $a = 1$ and $\xi = 2$, we find from (3) that $\Delta = 0$. When $a = 1$, it is readily verified that the set corresponding to the third type of motion includes the straight segments [$\xi = 2, 0 < \eta < (3E^4 - 4E^2 + 1)/(E^2(E^2 - 1))$] (Ref. 4) (for photons, $\xi = 2, 0 < \eta < 3$, by analogy with Refs. 5 and 6). It can also be shown that the function $\eta(\xi)$ has one maximum and $r(\xi)$ is a monotonically decreasing function.⁴ Thus, the set of constants corresponding to the first type of motion is bounded by the curve $\eta(\xi)$ for $\eta > 0$, as shown in Figs. 1 and 2. It is also readily shown that, when $\eta < 0$ and when η and ξ are such that the motion of the particle is possible, i.e.,

$$- [a(E^2 - 1)^{1/2} E - |\xi|]^2 \leq \eta < 0, \quad |\xi| \leq a(E^2 - 1)^{1/2} E,$$

the particle is also captured² (this set is illustrated in Fig. 2).

3. UNBOUND MOTION OF PHOTONS

Chandrasekhar¹ has shown that the condition for capture of a particle in the equatorial plane is the inequality

$$6 \cos [\arccos(-a)/3 + 2\pi/3]$$

$$-a \leq \xi \leq 6 \cos [\arccos(-a)/3] - a. \quad (5)$$

Thus, the functions of $r(\xi)$ and $\eta(\xi)$ are defined only for values satisfying the inequalities (5). We also note that the function $\eta(\xi)$ is a maximum for $\xi = -2a, r(-2a) = 3(\eta(-2a) = 27)$. This can be veri-

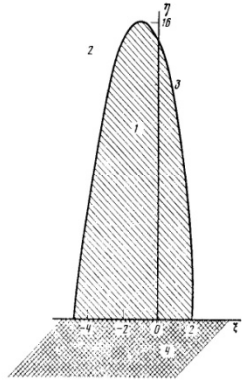


FIG. 1. Different types of particle motion for $E = 1$ and $a = 1$. Region 1—particle trapped, region 2—scattering; curve 3 corresponds to the third type of motion. Region 4 corresponds to values of the constants for which particle motion is impossible.

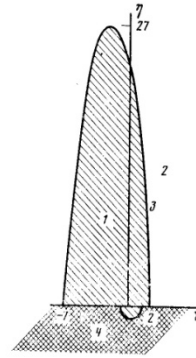


FIG. 2. Same as Fig. 1 for a massless particle and $a = 1$.

fied by direct evaluation of (3) and (4). Figure 2 shows a plot of the function $\eta(\xi)$ for $a = 1$.

4. MOTION OF PARTICLE OF ARBITRARY ENERGY

Consider a moving particle of arbitrary energy at infinity ($E > 1$). It can be verified that, if

$$\eta_{\max} = \frac{-(\alpha^2 - 18\alpha - 27) + (\alpha^4 + 28\alpha^2 + 270\alpha + 972\alpha + 729)^{1/2}}{2E^2\alpha}, \quad (6)$$

$$r_{\max} = (8\alpha^2/27 + \eta_{\max} E^2 \alpha (\alpha/3 + 1))^{1/2} - 2\alpha/3,$$

$$\xi_{\max} = 2a / (r_{\max} - 2),$$

where $\alpha = (E^2 - 1)^{-1}$, these values ensure that $R(r)$ and $\partial R / \partial r$ vanish, i.e., they satisfy (3). We also note that, for values chosen in accordance with (6), the right-hand side of the first equation in (4) vanishes, i.e., these values correspond to the maximum of $\eta(\xi)$. The values η_{\max} and r_{\max} turn out to be equal to the corresponding values of these quantities for $a = 0$ (Schwarzschild metric).⁷

5. ONE CASE OF UNBOUND PARTICLE MOTION

Consider a case of unbound particle motion for $E = 1$. If the motion takes place in the equatorial plane, $\eta = 0$ (Ref. 8) and

$$R(r) = 2r^2 - \xi^2 r^2 + 2(a - \xi)^2 r. \quad (7)$$

The motion then belongs to the third type if $\xi^4 = 16(a - \xi)^2$, and $r = \xi^2/4$. It follows that there are only two values that correspond to the third type of motion in the equatorial plane, namely, $\xi = -2 - 2(1 + a)^{1/2}$ and $\xi = 2 + 2(1 - a)^{1/2}$. Thus, the domain of definition of $\eta(\xi)$ is the segment $[-2(1 + (1 + a)^{1/2}), 2(1 + (1 - a)^{1/2})]$. The domain of variation of the function $r(\xi)$ is the segment $[(1 + (1 - a)^{1/2})^2, (1 + (1 + a)^{1/2})^2]$. This follows from the fact that $r(\xi)$ is a monotonically decreasing function of ξ . When $a = 0$, we find that $\eta(\xi) = 16 - \xi^2$. When $E \rightarrow 1$, we

Measuring the black hole parameters in the Galactic Center with Radioastron

- Let us consider an illumination of black holes. Then retro-photons form caustics around black holes or mirages around black holes or boundaries around shadows.
- (Zakharov, Nucita, DePaolis, Ingrosso,
- *New Astronomy* 10 (2005) 479; astro-ph/0411511)

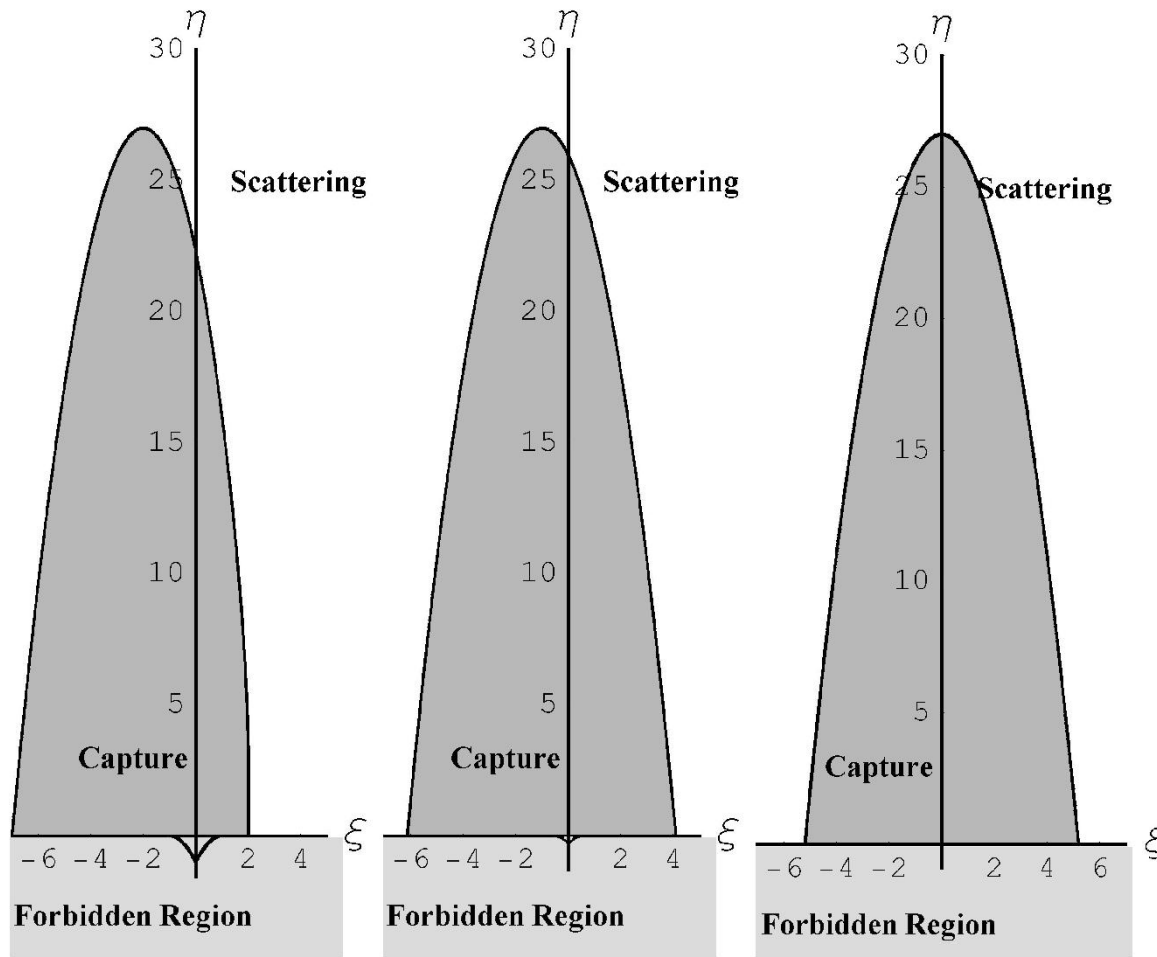


Fig. 1. Different types for photon trajectories and spin parameters ($a = 1., a = 0.5, a = 0.$). Critical curves separate capture and scatter regions. Here we show also the forbidden region corresponding to constants of motion $\eta < 0$ and $(\xi, \eta) \in M$ as it was discussed in the text.



INTERNATIONAL SERIES OF
MONOGRAPHS ON PHYSICS 69

The
Mathematical Theory
of Black Holes

S. Chandrasekhar

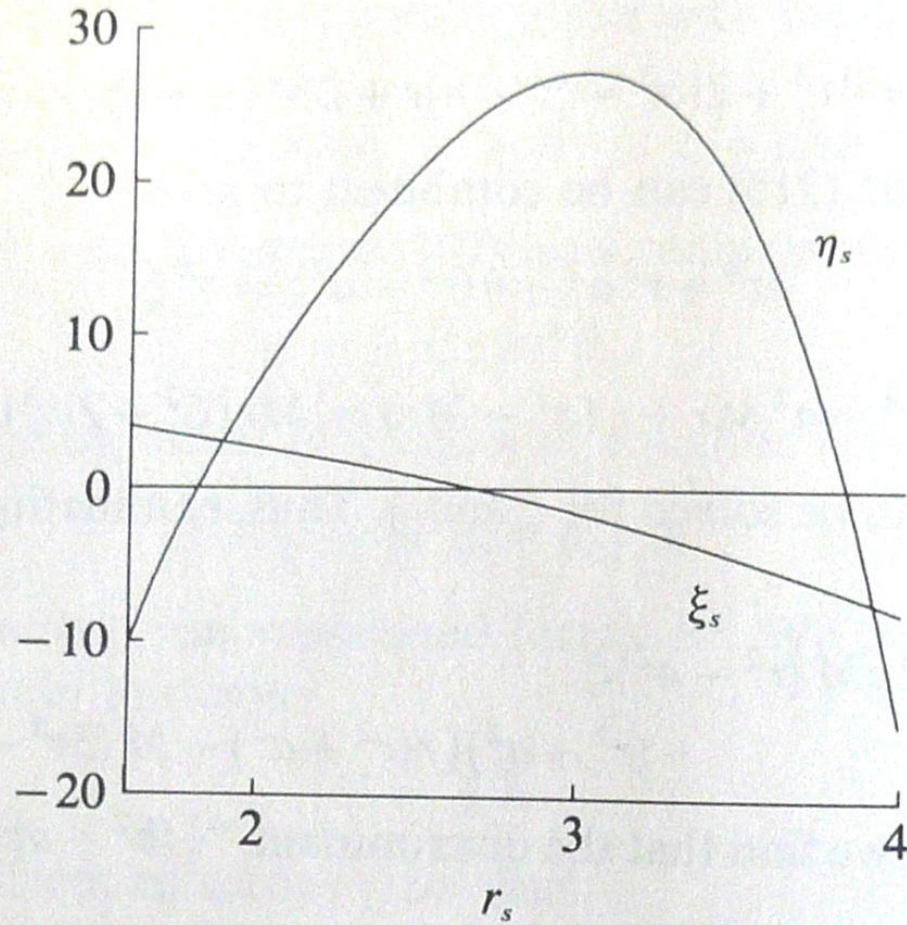


FIG. 34. The locus (ξ_s, η_s) determining the constants of the motion for three-dimensional orbits of constant radius described around a Kerr black-hole with $a = 0.8$. The unit of length along the abscissa is M .

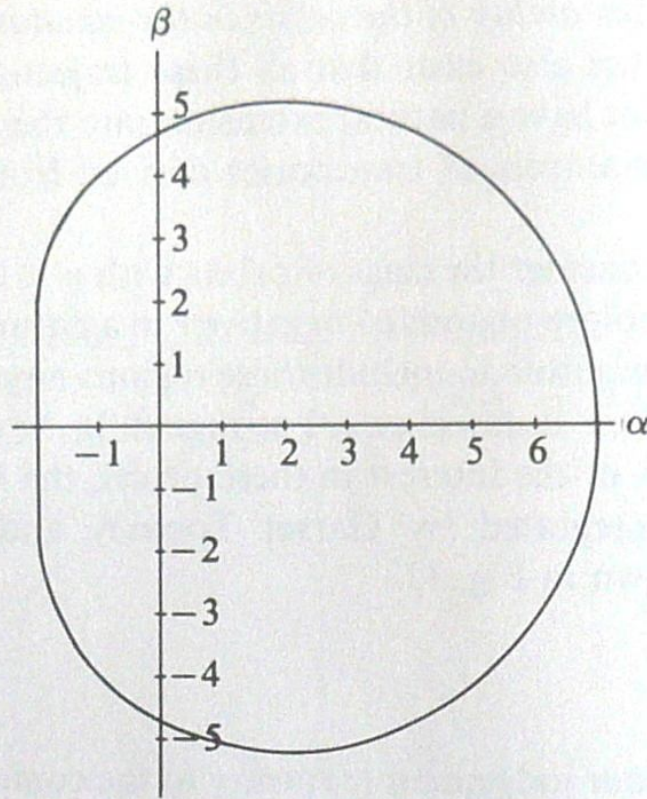


FIG. 38. The apparent shape of an extreme ($a = M$) Kerr black-hole as seen by a distant observer in the equatorial plane, if the black hole is in front of a source of illumination with an angular size larger than that of the black hole. The unit of length along the coordinate axes α and β (defined in equation (241)) is M .

black hole from infinity, the apparent shape will be determined by

$$(\alpha, \beta) = [\xi, \sqrt{\eta(\xi)}]. \quad (242)$$

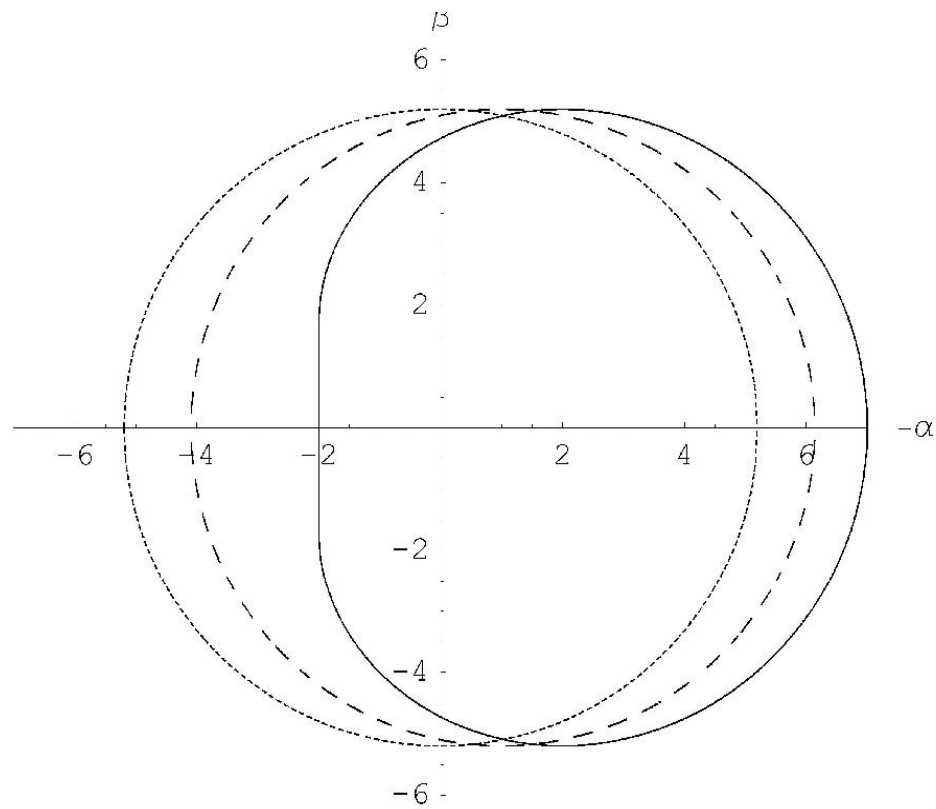


Fig. 2. Mirages around black hole for equatorial position of distant observer and different spin parameters. The solid line, the dashed line and the dotted line correspond to $a = 1, a = 0.5, a = 0$ correspondingly

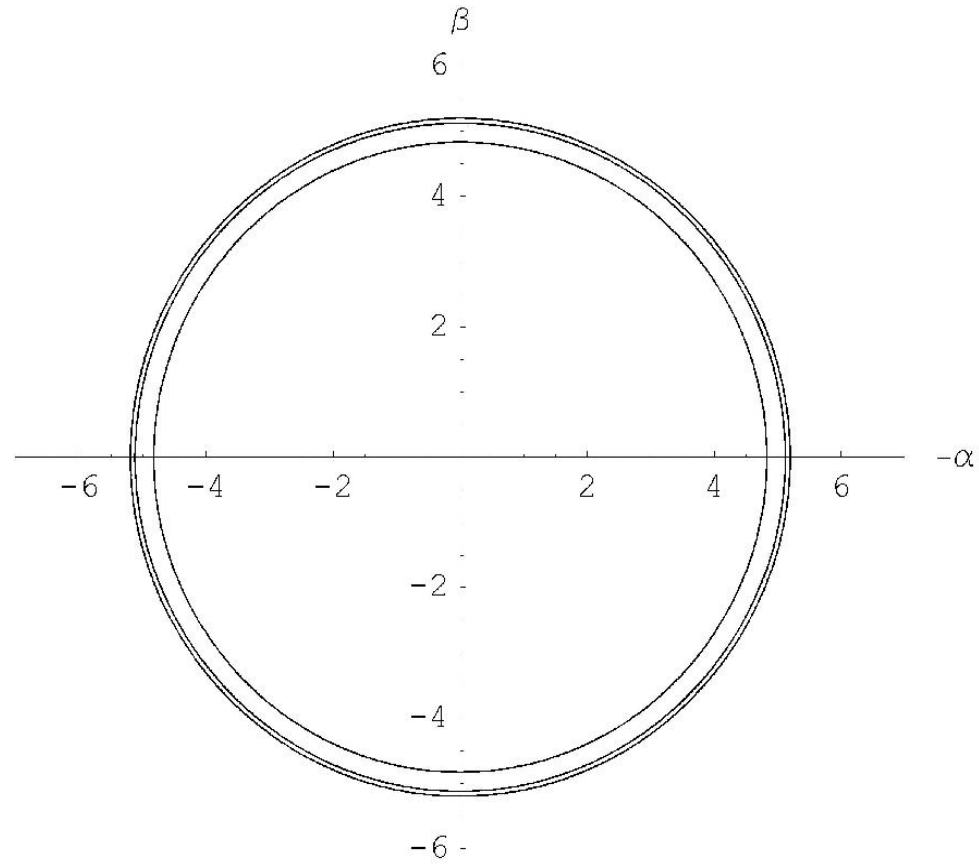


Fig. 3. Mirages around a black hole for the polar axis position of distant observer and different spin parameters ($a = 0, a = 0.5, a = 1$). Smaller radii correspond to greater spin parameters.

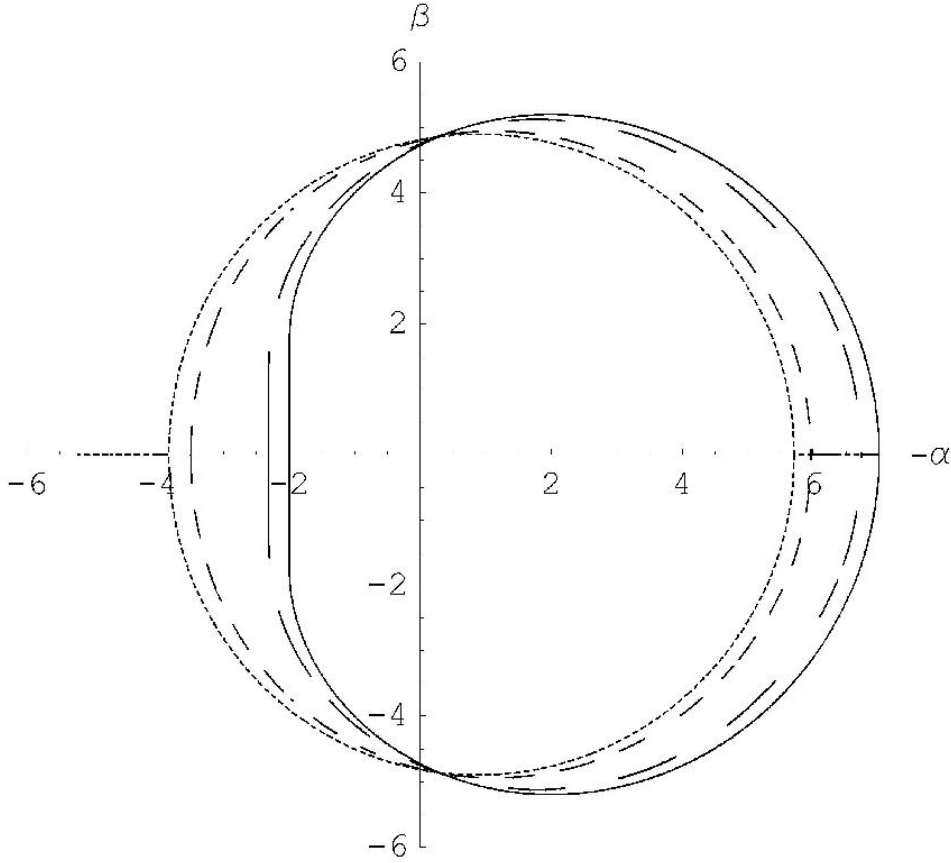


Fig. 5. Mirages around black hole for different angular positions of a distant observer and the spin $a = 1$. Solid, long dashed, short dashed and dotted lines correspond to $\theta_0 = \pi/2, \pi/3, \pi/6$ and $\pi/8$, respectively.

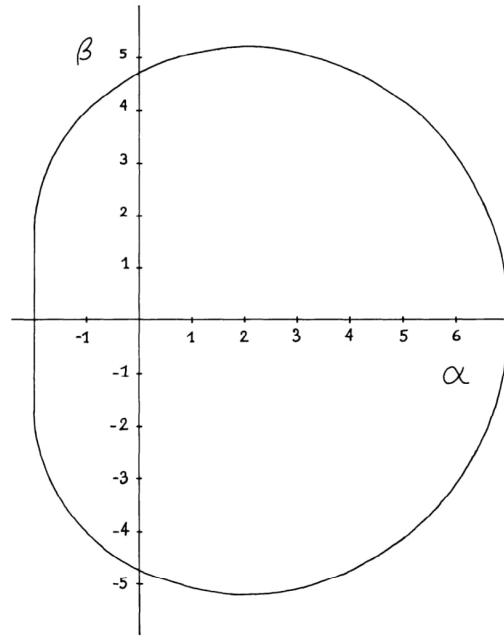


Figure 6. The apparent shape of an extreme ($a = m$) Kerr black hole as seen by a distant observer in the equatorial plane, if the black hole is in front of a source of illumination with an angular size larger than that of the black hole.

is largest there and because of the gravitational focusing effects associated with the bending of the rays toward the equatorial plane. Note that the radiation comes out along the flat portion of the apparent boundary of the extreme black hole as plotted in Figure 6.

D. Geometrical Optics

A detailed calculation of the brightness distribution coming from a source near a Kerr black hole requires more of geometrical optics than the calculation of photon trajectories. I will now review some techniques which are useful in making astrophysical calculations in connection with black holes.

The fundamental principle can be expressed as the conservation of photon density in phase space along each photon trajectory. A phase space element $d^3x d^3p$, the product of a proper spatial volume element and a physical momentum-space volume element in a local observer's frame of reference, is a Lorentz invariant, so the particular choice of local observer is arbitrary. The density $N(x^\alpha, p^{(\beta)})$ is defined

James Maxwell Bardeen passed
away on June 20, 2022



John Bardeen (1908 -1991), the father of J. M. Bardeen.
E. Wigner was J. Bardeen' supervisor



Direct Measurements of Black Hole Charge with Future Astrometrical Missions

A.F. Zakharov^{1,2,3}, F. De Paolis⁴, G. Ingrosso⁴, A.A. Nucita⁴

¹ Institute of Theoretical and Experimental Physics, 25, B.Chermushkinskaya st., Moscow, 117259, Russia,

² Astro Space Centre of Lebedev Physics Institute, 84/32, Profsoyuznaya st., Moscow, 117810, Russia,

³ Joint Institute for Nuclear Research, Dubna, Russia

⁴ Department of Physics, University of Lecce and INFN, Section of Lecce, Via Arnesano, I-73100 Lecce, Italy

Received / accepted

Abstract. Recently, Zakharov et al. (2005a) considered the possibility of evaluating the spin parameter and the inclination angle for Kerr black holes in nearby galactic centers by using future advanced astrometrical instruments. A similar approach which uses the characteristic properties of gravitational retro-lensing images can be followed to measure the charge of Reissner-Nordström black hole. Indeed, in spite of the fact that their formation might be problematic, charged black holes are objects of intensive investigations. From the theoretical point of view it is well-known that a black hole is described by only three parameters, namely, its mass M , angular momentum J and charge Q . Therefore, it would be important to have a method for measuring all these parameters, preferably by model independent way. In this paper, we propose a procedure to measure the black hole charge by using the size of the retro-lensing images that can be revealed by future astrometrical missions. A discussion of the Kerr-Newmann black hole case is also offered.

$$R(r_{max}) = 0, \quad \frac{\partial R}{\partial r}(r_{max}) = 0, \quad (6)$$

as it was done, for example, by Chandrasekhar (1983) to solve similar problems.

Introducing the notation $\xi^2 = l$, $Q^2 = q$, we obtain

$$R(r) = r^4 - lr^2 + 2lr - qr. \quad (7)$$

The discriminant Δ of the polynomial $R(r)$ has the form (as it was shown by Zakharov (1991a,b, 1994a)):

$$\Delta = 16l^3[l^2(1 - q) + l(-8q^2 + 36q - 27) - 16q^3]. \quad (8)$$

The polynomial $R(r)$ thus has a multiple root if and only if

$$l^3[l^2(1 - q) + l(-8q^2 + 36q - 27) - 16q^3] = 0. \quad (9)$$

Excluding the case $l = 0$, which corresponds to a multiple root at $r = 0$, we find that the polynomial $R(r)$ has a multiple root for $r \geq r_+$ if and only if

$$l^2(1 - q) + l(-8q^2 + 36q - 27) - 16q^3 = 0. \quad (10)$$

If $q = 0$, we obtain the well-known result for a Schwarzschild black hole (Misner, Thorne and Wheeler 1973; Wald 1984; Lightman et al. 1975), $l = 27$, or $L_{cr} = 3\sqrt{3}$. If $q = 1$, then $l = 16$, or $L_{cr} = 4$, which also corresponds to numerical results given by Young (1976).

The photon capture cross section for an extreme charged black hole turns out to be considerably smaller than the capture cross section of a Schwarzschild black hole. The critical value of the impact parameter, characterizing the capture cross section for a Reissner - Nordström black hole, is determined by the equation (Zakharov 1991a,b, 1994a)

$$l = \frac{(8q^2 - 36q + 27) + \sqrt{(8q^2 - 36q + 27)^2 + 64q^3(1 - q)}}{2(1 - q)}. \quad (11)$$

Table 1. The fringe sizes (in micro arcseconds) for the standard and advanced apogees B_{\max} (350 000 and 3 200 000 km, respectively).

$B_{\max}(\text{km}) \setminus \lambda(\text{cm})$	92	18	6.2	1.35
3.5×10^5	540	106	37	8
3.2×10^6	59	12	4	0.9

4. The space RADIOASTRON interferometer

The space-based radio telescope RADIOASTRON¹ is planned to be launched within few next years². This space-based 10-m radio telescope will be used for space – ground VLBI observations. The measurements will have extremely high angular resolutions, namely about 1–10 μas (in particular about 8 μas at the shortest wavelength of 1.35 cm and a standard orbit³, and could be about 0.9 μas for the high orbit configuration at the same wavelength. Four wave bands will be used corresponding to $\lambda = 1.35$ cm, $\lambda = 6.2$ cm, $\lambda = 18$ cm, $\lambda = 92$ cm (see Table 1). A detailed calculation of the high-apogee evolving orbits (B_{\max}) can be done, once the exact launch time is known.

After several years of observations, it should be possible to move the spacecraft to a much higher orbit (with apogee radius about 3.2 million km), by additional spacecraft maneuvering using the gravitational force of the Moon. The fringe sizes (in μas) for the apogee of the above-mentioned orbit and for all RADIOASTRON wavelengths are given in Table 1.

By comparing Figs. 1, 2 and Table 1, one can see that there are non-negligible chances to observe such mirages around the black hole at the Galactic Center and in nearby AGNs and microquasars in the radio-band using RADIOASTRON facilities.

We also mention that this high resolution in radio band will be achieved also by Japanese VLBI project VERA (VLBI Exploration of Radio Astrometry), since the angular resolution aimed at will be at the 10 μas level (Sawad-Satoh 2000; Honma 2001). Therefore, the only problem left is to have a powerful enough radio source to illuminate a black hole in order to have retro-lensing images detectable by such radio VLBI telescopes as RADIOASTRON or VERA.

¹ See web-site <http://www.asc.rssi.ru/radioastron/> for more information.

² This project was proposed by the Astro Space Center (ASC) of Lebedev Physical Institute of the Russian Academy of Sciences (RAS) in collaboration with other institutions of RAS and RosAviaKosmos. Scientists from 20 countries are developing the scientific payload for the satellite by providing by ground-based support to the mission.

³ The satellite orbit will have high apogee, and its rotation period around Earth will be 9.5 days, which evolves as a result of the weak gravitational perturbations from the Moon and the Sun. The perigee has been planned to be between 10^4 and 7×10^4 km and the apogee between 310 and 390 thousand kilometers. The basic orbit parameters will be the following: the orbital period is $P = 9.5$ days, the semi-major axis is $a = 189\,000$ km, the eccentricity is $e = 0.853$, the perigee is $H = 29\,000$ km.

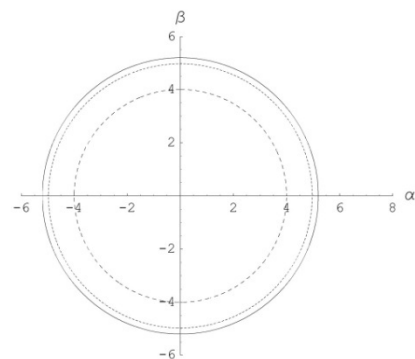


Fig. 1. Shadow (mirage) sizes are shown for selected charges of black holes $Q = 0$ (solid line), $Q = 0.5$ (short dashed line), and $Q = 1$ (long dashed line).

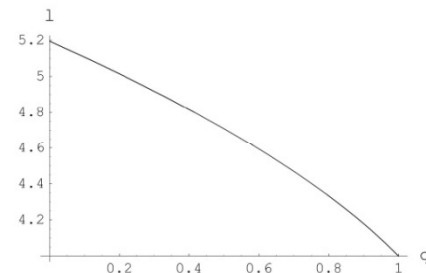


Fig. 2. The mirage radius l is shown as a function of the black hole charge q (l and q are given in units of M).

5. Searches for mirages near Sgr A* with RADIOASTRON

Radio, near-infrared, and X-ray spectral band observations are developing very rapidly (Lo et al. 1998, 1999; Genzel et al. 2003; Ghez et al. 2004; Baganoff et al. 2001, 2003; Bower et al. 2002, 2003; Narayan 2003; Bower et al. 2004)⁴, and it is known that Sgr A* harbors the closest massive black hole with mass estimated to be $4.07 \times 10^6 M_{\odot}$ (Bower et al. 2004; Melia & Falcke 2001; Ghez et al. 2003; Schodel et al. 2003).

Following the idea of Falcke et al. (2000) and of Zakharov et al. (2005a,b,c,d) we propose to use the VLBI technique to observe mirages around massive black holes and, in particular, towards the black hole at Galactic Center. To evaluate the shadow shape Falcke et al. (2000) used the ray-tracing technique. The boundaries of the shadows are black hole mirages.

⁴ An interesting idea to use radio pulsars to investigate the region nearby black hole horizon was proposed recently by Pfahl & Loeb (2003).

Constraints on a charge in the Reissner-Nordström metric for the black hole at the Galactic Center

Alexander F. Zakharov*

North Carolina Central University, Durham, North Carolina 27707, USA; Institute of Theoretical and Experimental Physics, Moscow 117218, Russia; Joint Institute for Nuclear Research, Dubna 141980, Russia; Institute for Computer Aided Design of RAS, 123056 Moscow, Russia; and National Research Nuclear University (NRNU MEPhI), 115409 Moscow, Russia
(Received 5 March 2013; published 9 September 2014)

Using an algebraic condition of vanishing discriminant for multiple roots of fourth-degree polynomials, we derive an analytical expression of a shadow size as a function of a charge in the Reissner-Nordström (RN) metric [1,2]. We consider shadows for negative tidal charges and charges corresponding to naked singularities $q = Q^2/M^2 > 1$, where Q and M are black hole charge and mass, respectively, with the derived expression. An introduction of a negative tidal charge q can describe black hole solutions in theories with extra dimensions, so following the approach we consider an opportunity to extend the RN metric to negative Q^2 , while for the standard RN metric Q^2 is always non-negative. We found that for $q > 9/8$, black hole shadows disappear. Significant tidal charges $q = -6.4$ (suggested by Bin-Nun [3–5]) are not consistent with observations of a minimal spot size at the Galactic Center observed in mm-band; moreover, these observations demonstrate that a Reissner-Nordström black hole with a significant charge $q \approx 1$ provides a better fit of recent observational data for the black hole at the Galactic Center in comparison with the Schwarzschild black hole.

DOI: 10.1103/PhysRevD.90.062007

PACS numbers: 04.80.Cc, 04.20.-q, 04.50.Gh, 04.70.Bw

I. INTRODUCTION

Soon after the discovery of general relativity (GR), the first solutions corresponding to spherical symmetric black holes were found [1,2,6]; however, initially people were rather sceptical about possible astronomical applications of the solutions corresponding to black holes [7] (see also, for instance, one of the first textbooks on GR [8]). Even after an introduction to the black hole concept by Wheeler [9] (he used the term in his public lecture in 1967 [10]), we did not know too many examples where we really need GR models with strong gravitational fields that arise near black hole horizons to explain observational data. The cases where we need strong field approximation are very important since they give an opportunity to check GR predictions in a strong field limit; therefore, one could significantly constrain alternative theories of gravity.

One of the most important options to test gravity in the strong field approximation is analysis of relativistic line shape as it was shown in [11], with assumptions that a line emission is originated at a circular ring area of a flat accretion disk. Later on, such signatures of the Fe $K\alpha$ line have been found in the active galaxy MCG-6-30-15 [12]. Analyzing the spectral line shape, the authors concluded the emission region is so close to the black hole horizon that one has to use Kerr metric approximation [13] to fit observational data [12]. Results of simulations of iron $K\alpha$ line formation are given in [14,15] (where we used our

approach [16]); see also [17] for a more recent review of the subject.

Now there are two basic observational techniques to investigate a gravitational potential at the Galactic Center, namely, (a) monitoring the orbits of bright stars near the Galactic Center to reconstruct a gravitational potential [18] (see also a discussion about an opportunity to evaluate black hole dark matter parameters in [19] and an opportunity to constrain some class of an alternative theory of gravity [20]) and (b) measuring in mm band, with VLBI technique, the size and shape of shadows around the black hole, giving an alternative possibility to evaluate black hole parameters. The formation of retro-lensing images (also known as mirages, shadows, or “faces” in the literature) due to the strong gravitational field effects nearby black holes has been investigated by several authors [21–24].

Theories with extra dimensions admit astrophysical objects (supermassive black holes in particular) which are rather different from standard ones. Tests have been proposed when it would be possible to discover signatures of extra dimensions in supermassive black holes since the gravitational field may be different from the standard one in the GR approach. So, gravitational lensing features are different for alternative gravity theories with extra dimensions and general relativity.

Recently, Bin-Nun [3–5] discussed the possibility that the black hole at the Galactic Center is described by the tidal Reissner-Nordström metric which may be admitted by the Randall-Sundrum II braneworld scenario [25]. Bin-Nun suggested an opportunity of evaluating the black hole

*zakharov@itep.ru

$$\text{Dis}(s_1, s_2, s_3, s_4) = \begin{vmatrix} 1 & 1 & 1 & 1 \\ X_1 & X_2 & X_3 & X_4 \\ X_1^2 & X_2^2 & X_3^2 & X_4^2 \\ X_1^3 & X_2^3 & X_3^3 & X_4^3 \end{vmatrix} = \begin{vmatrix} 4 & p_1 & p_2 & p_3 \\ p_1 & p_2 & p_3 & p_4 \\ p_2 & p_3 & p_4 & p_5 \\ p_3 & p_4 & p_5 & p_6 \end{vmatrix}. \quad (20)$$

Expressing the polynomials p_k ($1 \leq k \leq 6$) in terms of the polynomials s_k ($1 \leq k \leq 4$) and using Newton's equations

$$\text{Dis}(s_1, s_2, s_3, s_4) = \begin{vmatrix} 4 & 0 & 2l & -6l \\ 0 & 2l & -6l & 2l(l+2q) \\ 2l & -6l & 2l(l+2q) & -10l^2 \\ -6l & 2l(l+2q) & -10l^2 & 2l^2(l+6+3q) \end{vmatrix} = 16l^3[l^2(1-q) + l(-8q^2 + 36q - 27) - 16q^3]. \quad (22)$$

The polynomial $R(r)$ thus has a multiple root if and only if

$$l^3[l^2(1-q) + l(-8q^2 + 36q - 27) - 16q^3] = 0. \quad (23)$$

Excluding the case $l = 0$, which corresponds to a multiple root at $r = 0$, we find that the polynomial $R(r)$ has a multiple root for $r \geq r_+$ if and only if

$$l^2(1-q) + l(-8q^2 + 36q - 27) - 16q^3 = 0. \quad (24)$$

If $q = 0$, we obtain the well-known result for a Schwarzschild black hole [38,39,49], $l_{\text{cr}} = 27$, or $\xi_{\text{cr}} = 3\sqrt{3}$ [where l_{cr} is the positive root of Eq. (24)]. If $q = 1$, then $l = 16$, or $\xi_{\text{cr}} = 4$, which also corresponds to numerical results given in paper [50]. The photon capture cross section for an extreme charged black hole turns out to be considerably smaller than the capture cross section of a Schwarzschild black hole. The critical value of the impact parameter, characterizing the capture cross section for a RN black hole, is determined by the equation

$$l_{\text{cr}} = \frac{(8q^2 - 36q + 27) + \sqrt{D_1}}{2(1-q)}, \quad (25)$$

where $D_1 = (8q^2 - 36q + 27)^2 + 64q^3(1-q) = -512(q - \frac{9}{8})^3$. It is clear from the last relation that there are circular unstable photon orbits only for $q \leq \frac{9}{8}$ (see also results in [37] about the same critical value). Substituting Eq. (25) into the expression for the coefficients of the polynomial $R(r)$ it is easy to calculate the radius of the unstable circular photon orbit (which is the same as the minimum periastron

distance). The orbit of a photon moving from infinity with the critical impact parameter, determined in accordance with Eq. (25) spirals into circular orbit. To find a radius of photon unstable orbit we will solve Eq. (7) substituting l_{cr} in the relation. From trigonometric formula for roots of cubic equation we have

$$\begin{aligned} p_1 = s_1 = 0, \quad p_2 = -2s_2, \quad p_3 = 3s_3, \\ p_4 = 2s_2^3 - 4s_4, \quad p_5 = -5s_3s_2, \\ p_6 = -2s_2^3 + 3s_3^2 + 6s_4s_2, \end{aligned} \quad (21)$$

where $s_1 = 0, s_2 = -l, s_3 = -2l, s_4 = -ql$, corresponding to the polynomial $R(r)$ in Eq. (8). The discriminant Dis of the polynomial $R(r)$ has the form

distance). The orbit of a photon moving from infinity with the critical impact parameter, determined in accordance with Eq. (25) spirals into circular orbit. To find a radius of photon unstable orbit we will solve Eq. (7) substituting l_{cr} in the relation. From trigonometric formula for roots of cubic equation we have

$$r_{\text{crit}} = 2\sqrt{\frac{l_{\text{cr}}}{6}} \cos \frac{\alpha}{3}, \quad (26)$$

where

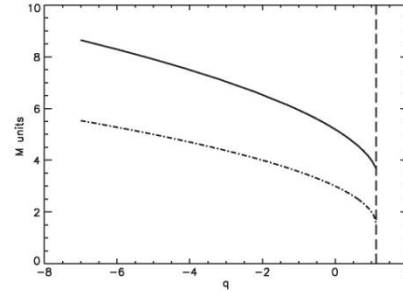


FIG. 1. Shadow (mirage) radius (solid line) and radius of the last circular unstable photon orbit (dot-dashed line) in M units as a function of q . The critical value $q = 9/8$ is shown with dashed vertical line.

Jourdain: “For more than forty years I have been speaking prose while knowing nothing of it,” (from “*Bourgeois Gentleman* or *The Middle-Class Aristocrat* “, J. B. Moliere)

We: “For many years we had speaking about BH’s in Randall --- Sundrum model or in (beyond) Horndesky theory (scalar-tensor one) while knowing nothing of the theories...” (tidal charge or “charge” due to scalar-tensor theories)

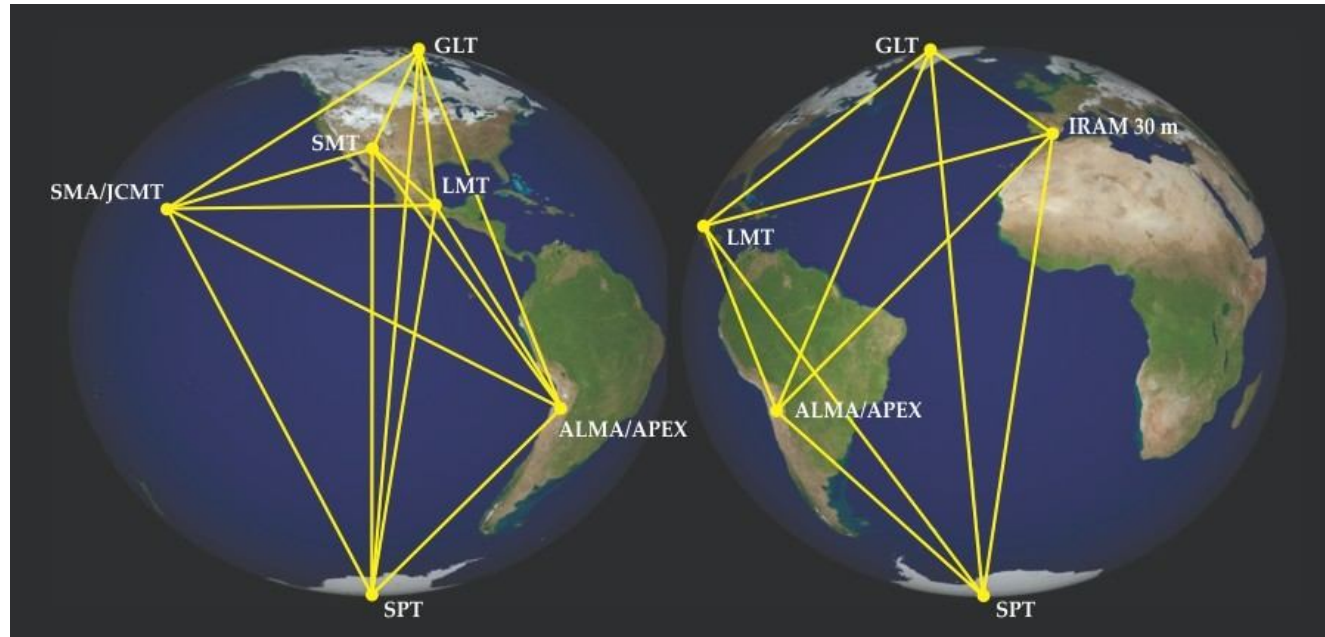
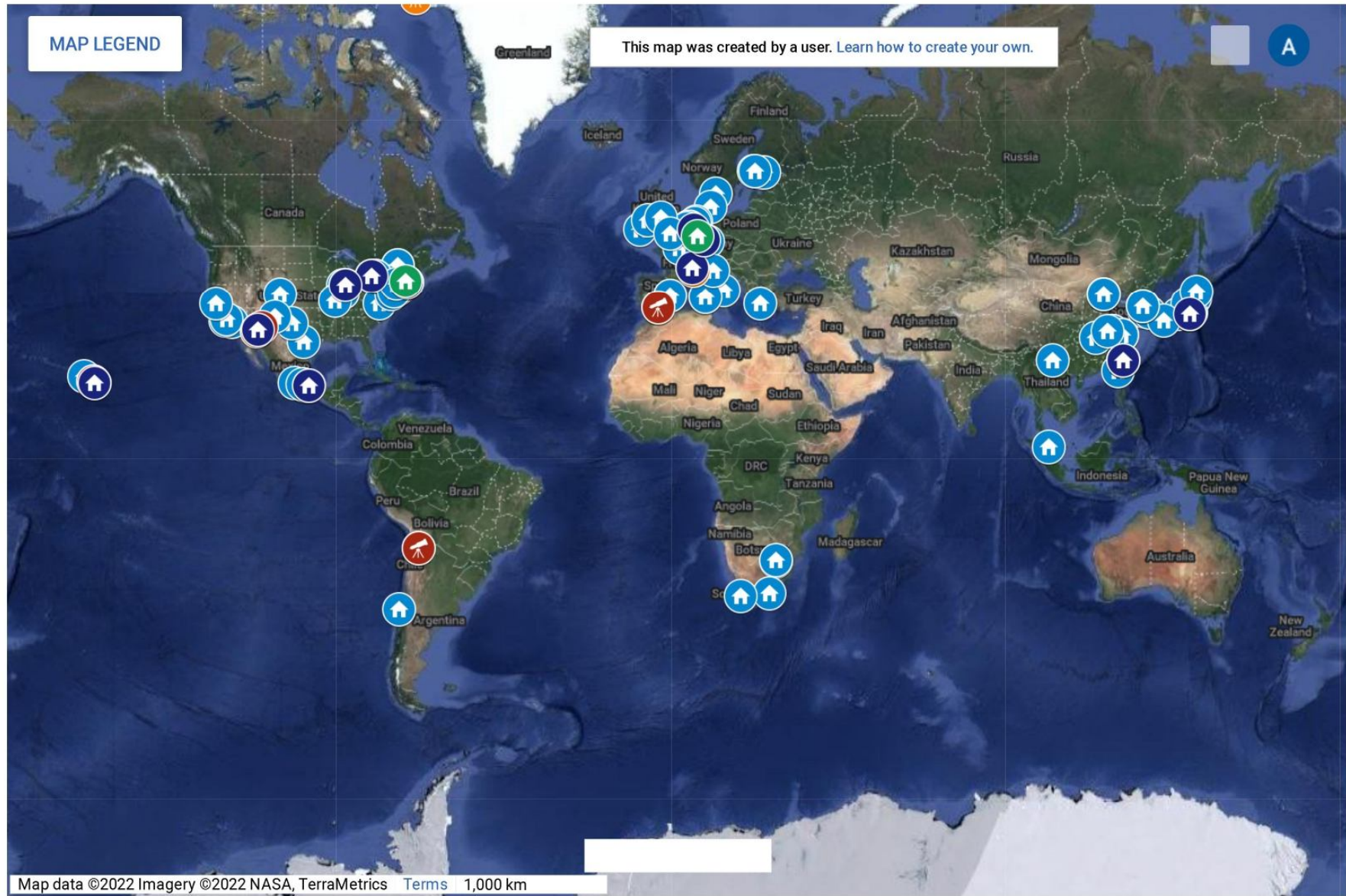


Figure 2. **The Event Horizon Telescope** is a global array of millimeter telescopes (see <http://eventhorizontelescope.org/array>) that aims to take the first pictures of black holes. (Courtesy of Dan Marrone/University of Arizona.)

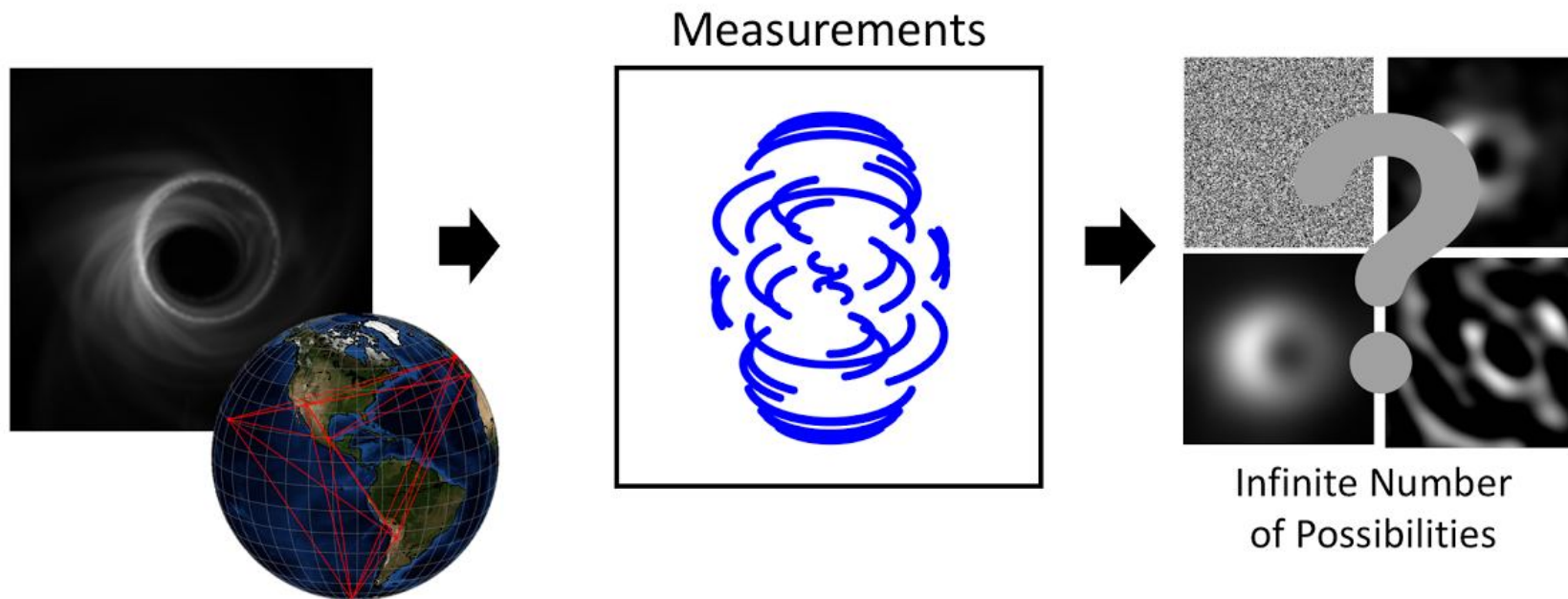
Published in: Dimitrios Psaltis; Feryal Özel; *Physics Today* **2018**, 71, 70-71.

DOI: 10.1063/PT.3.3906

Copyright © 2018 American Institute of Physics



EHT team: “Similarly, for the EHT, the data we take only tells us only a piece of the story, as there are an infinite number of possible images that are perfectly consistent with the data we measure. But not all images are created equal— some look more like what we think of as images than others. To chose the best image, we essentially take all of the infinite images that explain our telescope measurements, and rank them by how reasonable they look. We then choose the image (or set of images) that looks most reasonable. ”



Constraints on black-hole charges with the 2017 EHT observations of M87*

Prashant Kocherlakota¹, Luciano Rezzolla,¹⁻³ Heino Falcke,⁴ Christian M. Fromm,^{5,6,1} Michael Kramer,⁷ Yosuke Mizuno,^{8,9} Antonios Nathanail,^{9,10} Héctor Olivares,¹¹ Ziri Younsi,^{11,3} Kazunori Akiyama,^{12,13,5} Antxon Alberdi,¹⁴ Walter Alef,⁷ Juan Carlos Algaba,¹⁵ Richard Anantua,^{5,6,16} Keiichi Asada,¹⁷ Rebecca Azulay,^{18,19,7} Anne-Kathrin Baczo,⁷ David Ball,²⁰ Mislav Baloković,^{5,6} John Barrett,¹² Bradford A. Benson,^{21,22} Dan Bintley,²³ Lindy Blackburn,^{5,6} Raymond Blundell,⁶ Wilfred Boland,²⁴ Katherine L. Bouman,^{5,6,25} Geoffrey C. Bower,²⁶ Hope Boyce,^{27,28} Michael Bremer,²⁹ Christiaan D. Brinkerink,⁴ Roger Brissenden,^{5,6} Silke Britzen,⁷ Avery E. Broderick,³⁰⁻³² Dominique Brogiere,²⁹ Thomas Bronzwaer,⁴ Do-Young Byun,^{33,34} John E. Carlstrom,^{35,22,36,37} Andrew Chael,^{38,39} Chi-kwan Chan,^{20,40} Shami Chatterjee,⁴¹ Koushik Chatterjee,⁴² Ming-Tang Chen,²⁶ Yongjun Chen (陈永军),^{43,44} Paul M. Chesler,⁵ Ilje Cho,^{33,34} Pierre Christian,⁴⁵ John E. Conway,⁴⁶ James M. Cordes,⁴¹ Thomas M. Crawford,^{47,23,5} Geoffrey B. Crew,¹² Alejandro Cruz-Orsorio,⁹ Yuzhu Cui,^{47,48} Jordy Davelaar,^{49,16,4} Mariafelicia De Laurentis,^{50,9,51} Roger Deane,⁵²⁻⁵⁴ Jessica Dempsey,²³ Gregory Desvignes,⁵⁵ Sheperd S. Doeleman,^{5,6} Ralph P. Eatough,^{56,7} Joseph Farah,^{6,5,57} Vincent L. Fish,¹² Ed Fomalont,⁵⁸ Raquel Fraga-Encinas,⁴ Per Friberg,²³ H. Alyson Ford,⁵⁹ Antonio Fuentes,¹⁴ Peter Galison,^{60,61} Charles F. Gammie,^{62,63} Roberto García,²⁹ Olivier Gentaz,²⁹ Boris Georgiev,^{31,32} Ciriaco Goddi,^{4,64} Roman Gold,^{65,30} José L. Gómez,¹⁴ Arturo I. Gómez-Ruiz,^{66,67} Minfeng Gu (顾敏峰),^{43,68} Mark Gurwell,⁶ Kazuhiro Hada,^{47,48} Daryl Haggard,^{27,28} Michael H. Hecht,¹² Ronald Hesper,⁶⁹ Luis C. Ho (何子山),^{70,71} Paul Ho,¹⁷ Mareki Honma,^{47,48,72} Chih-Wei L. Huang,¹⁷ Lei Huang (黄磊),^{43,68} David H. Hughes,⁶⁶ Shiro Ikeda,^{13,73-75} Makoto Inoue,¹⁷ Sara Issaoun,⁴ David J. James,^{5,6} Buell T. Jannuzi,²⁰ Michael Janssen,⁷ Britton Jeter,^{31,32} Wu Jiang (江楷),⁴³ Alejandra Jimenez-Rosales,⁴ Michael D. Johnson,^{5,6} Svetlana Jorstad,^{76,7} Taehyun Jung,^{33,34} Mansour Karami,^{30,31} Ramesh Karuppusamy,⁷ Tomohisa Kawashima,⁷⁸ Garrett K. Keating,⁶ Mark Kettenis,⁷⁹ Dong-Jin Kim,⁷ Jae-Young Kim,^{33,7} Jongsoo Kim,³³ Junhan Kim,^{20,25} Motoki Kino,^{13,80} Jun Yi Koay,¹⁷ Yutaro Kofuji,^{47,72} Patrick M. Koch,¹⁷ Shoko Koyama,¹⁷ Carsten Kramer,²⁹ Thomas P. Krichbaum,⁷ Cheng-Yu Kuo,^{81,17} Tod R. Lauer,⁸² Sang-Sung Lee,³³ Aviad Levis,²⁵ Yan-Rong Li (李彦荣),⁸³ Zhiyuan Li (李志远),^{84,85} Michael Lindqvist,⁴⁶ Rocco Lico,^{14,7} Greg Lindahl,⁶ Jun Liu (刘俊),⁷ Kuo Liu,⁷ Elisabetta Liuzzo,⁸⁶ Wen-Ping Lo,^{17,87} Andrei P. Lobanov,⁷ Laurent Loinard,^{88,89} Colin Lonsdale,¹² Ru-Sen Lu (路如森),^{43,44,7} Nicholas R. MacDonald,⁷ Jirong Mao (毛基荣),⁹⁰⁻⁹² Nicola Marchili,^{86,7} Sera Markoff,^{42,93} Daniel P. Marrone,²⁰ Alan P. Marscher,⁷⁶ Iván Martí-Vidal,^{18,19} Satoki Matsushita,¹⁷ Lynn D. Matthews,¹² Lia Medeiros,^{94,20} Karl M. Menten,⁷ Izumi Mizuno,²³ James M. Moran,^{5,6} Kotaro Moriyama,^{12,47} Monika Moscibrodzka,⁴ Cornelia Müller,^{7,4} Gibwa Musoke,^{42,4} Alejandro Mus Mejías,^{18,19} Hiroshi Nagai,^{13,48} Neil M. Nagar,⁹⁵ Masanori Nakamura,^{96,17} Ramesh Narayan,^{5,6} Gopal Narayanan,⁷ Iniyar Natarajan,⁹⁷ Joseph Neilsen,³⁹ Roberto Neri,²⁹ Chunhong Ni,^{31,32} Aristeidis Noutsos,⁷ Michael A. Nowak,¹⁰⁰ Hiroki Okino,^{47,72} Gisela N. Ortiz-León,⁷ Tomoaki Oyama,⁴⁷ Feryal Özel,²⁰ Daniel C. M. Palumbo,^{5,6} Jongho Park,¹⁷ Nimesh Patel,⁶ Ue-Li Pen,^{30,101-103} Dominic W. Pesce,^{5,6} Vincent Piétu,²⁹ Richard Plambeck,¹⁰⁴ Aleksandar PopStefanija,⁹⁷ Oliver Porth,^{42,9} Felix M. Pötzl,⁷ Ben Prather,⁶² Jorge A. Preciado-López,³⁰ Dimitrios Psaltis,²⁰ Hung-Yi Pu,^{105,17,30} Venkatesh Ramakrishnan,⁹⁸ Ramprasad Rao,²⁶ Mark G. Rawlings,²³ Alexander W. Raymond,^{5,6} Angelo Ricarte,^{5,6} Bart Ripperda,^{106,16} Freek Roelofs,⁴ Alan Rogers,¹² Eduardo Ros,⁷ Mel Rose,²⁰ Arash Roshanineshat,²⁰ Helge Rottmann,⁷ Alan L. Roy,⁷ Chet Ruzszyk,¹² Kazi L. J. Rygl,⁸⁶ Salvador Sánchez,¹⁰⁷ David Sánchez-Argüelles,^{66,67} Mahito Sasada,^{47,108} Tuomas Savolainen,^{109,110,7} F. Peter Schloerb,⁹⁷ Karl-Friedrich Schuster,²⁹ Lijing Shao,^{7,71} Zhiqiang Shen (沈志强),^{43,44} Des Small,⁷⁹ Bong Won Sohn,^{33,34,111} Jason SooHoo,¹² He Sun (孙赫),²⁵ Fumie Tazaki,⁴⁷ Alexandra J. Tetarenko,¹¹² Paul Tiede,^{31,32} Remo P. J. Tilanus,^{4,64,113,20} Michael Titus,¹² Kenji Toma,^{114,115} Pablo Torme,^{7,107} Tyler Trent,²⁰ Efthalia Traianou,⁷ Sascha Trippe,¹¹⁶ Ilse van Bemmell,⁷⁹ Huib Jan van Langevelde,^{79,117} Daniel R. van Rossum,⁴ Jan Wagner,⁷ Derek Ward-Thompson,¹¹⁸ John Wardle,¹¹⁹ Jonathan Weintraub,^{5,6} Norbert Wex,⁷ Robert Wharton,⁷ Maciek Wielgus,^{5,6} George N. Wong,⁶² Qingwen Wu (吴庆文),¹²⁰ Doosoo Yoon,⁴² André Young,⁴ Ken Young,⁶ Feng Yuan (袁峰),^{43,68,121} Ye-Fei Yuan (袁业飞),¹²² J. Anton Zensus,⁷ Guang-Yao Zhao,¹⁴ and Shan-Shan Zhao⁴³

(EHT Collaboration)

¹Institut für Theoretische Physik, Goethe-Universität, Max-von-Laue-Strasse 1, 60438 Frankfurt, Germany²Frankfurt Institute for Advanced Studies, Ruth-Moufang-Strasse 1, 60438 Frankfurt, Germany³School of Mathematics, Trinity College, Dublin 2, Ireland⁴Department of Astrophysics, Institute for Mathematics, Astrophysics and Particle Physics (IMAPP), Radboud University, P.O. Box 9010, 6500 GL Nijmegen, Netherlands⁵Black Hole Initiative at Harvard University, 20 Garden Street, Cambridge, Massachusetts 02138, USA

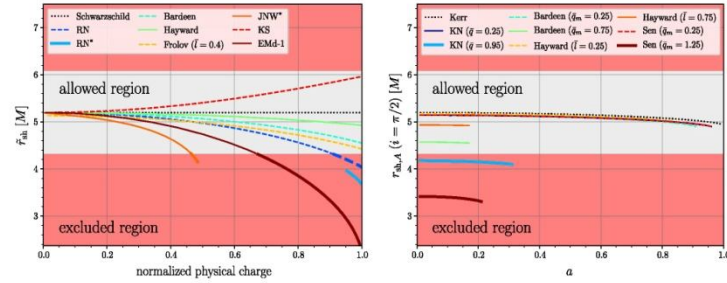


FIG. 2. Left: shadow radii r_{sh} for various spherically symmetric black-hole solutions, as well as for the JNW and RN naked singularities (marked with an asterisk), as a function of the physical charge normalized to its maximum value. The gray/red shaded regions refer to the areas that are $1-\sigma$ consistent/inconsistent with the 2017 EHT observations and highlight that the latter set constrains on the physical charges (see also Fig. 3 for the Emd-2 black hole). Right: shadow areal radii $r_{\text{sh},A}$ as a function of the dimensionless spin a for four families of black-hole solutions when viewed on the equatorial plane ($i = \pi/2$). Also in this case, the observations restrict the ranges of the physical charges of the Kerr-Newman and the Sen black holes (see also Fig. 3).

independent charges—can also produce shadow radii that are incompatible with the EHT observations; we will discuss this further below. The two Emd black-hole solutions (1 and 2) correspond to fundamentally different field contents, as discussed in [70].

We report in the right panel of Fig. 2 the shadow areal radius $r_{\text{sh},A}$ for a number of stationary black holes, such as Kerr [72], Kerr-Newman (KN) [73], Sen [74], and the rotating versions of the Bardeen and Hayward black holes [75]. The data refers to an observer inclination angle of $i = \pi/2$, and we find that the variation in the shadow size with spin at higher inclinations (of up to $i = \pi/100$) is at most about 7.1% (for $i = \pi/2$, this is 5%); of course, at zero-spin the shadow size does not change with inclination. The shadow areal radii are shown as a function of the dimensionless spin of the black hole $a := J/M^2$, where J is its angular momentum, and for representative values of the additional parameters that characterize the solutions. Note that—similar to the angular momentum for a Kerr black hole—the role of an electric charge or the presence of a de Sitter core (as in the case of the Hayward black holes) is to reduce the apparent size of the shadow. Furthermore, on increasing the spin parameter, we recover the typical trend that the shadow becomes increasingly noncircular, as encoded, e.g., in the distortion parameter δ_{sh} defined in [57,83] (see Appendix). Also in this case, while the regular rotating Bardeen and Hayward solutions are compatible with the present constraints set by the 2017 EHT observations, the Kerr-Newman and Sen families of black holes can produce shadow areal radii that lie outside of the $1-\sigma$ region allowed by the observations.

To further explore the constraints on the excluded regions for the Einstein-Maxwell-dilaton 2 and the Sen black holes, we report in Fig. 3 the relevant ranges for these two solutions. The Einstein-Maxwell-dilaton 2 black holes are nonrotating but have two physical charges expressed by the coefficients $0 < \tilde{q}_e < \sqrt{2}$ and $0 < \tilde{q}_m < \sqrt{2}$, while the Sen black holes spin (a) and have an additional electromagnetic charge \tilde{q}_m . Also in this case, the gray/red shaded regions refer to the areas that are consistent/inconsistent with the 2017 EHT observations. The figure shows rather easily that for these two black-hole families there are large

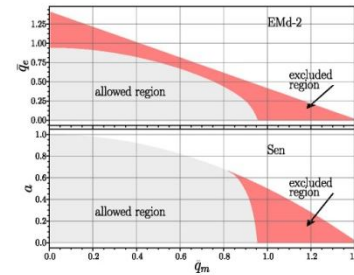
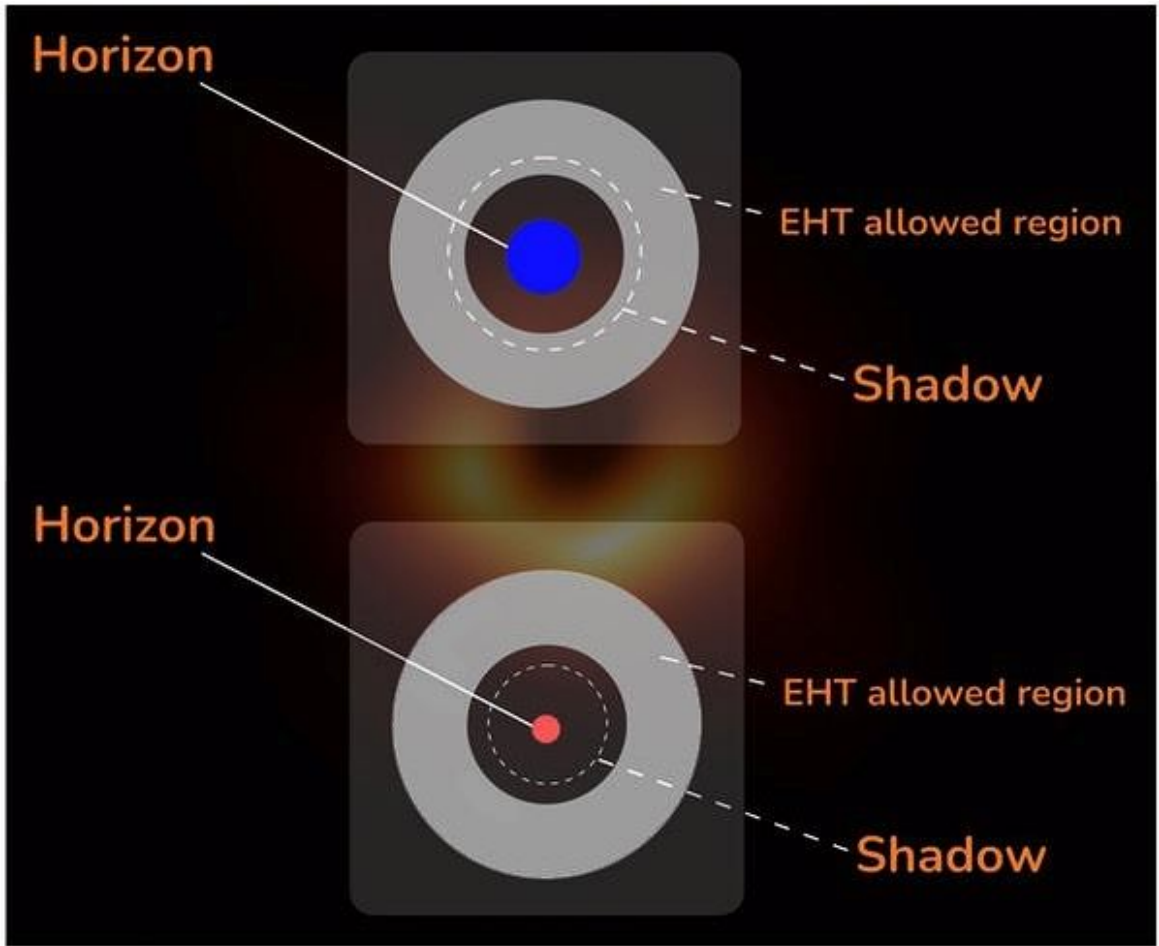
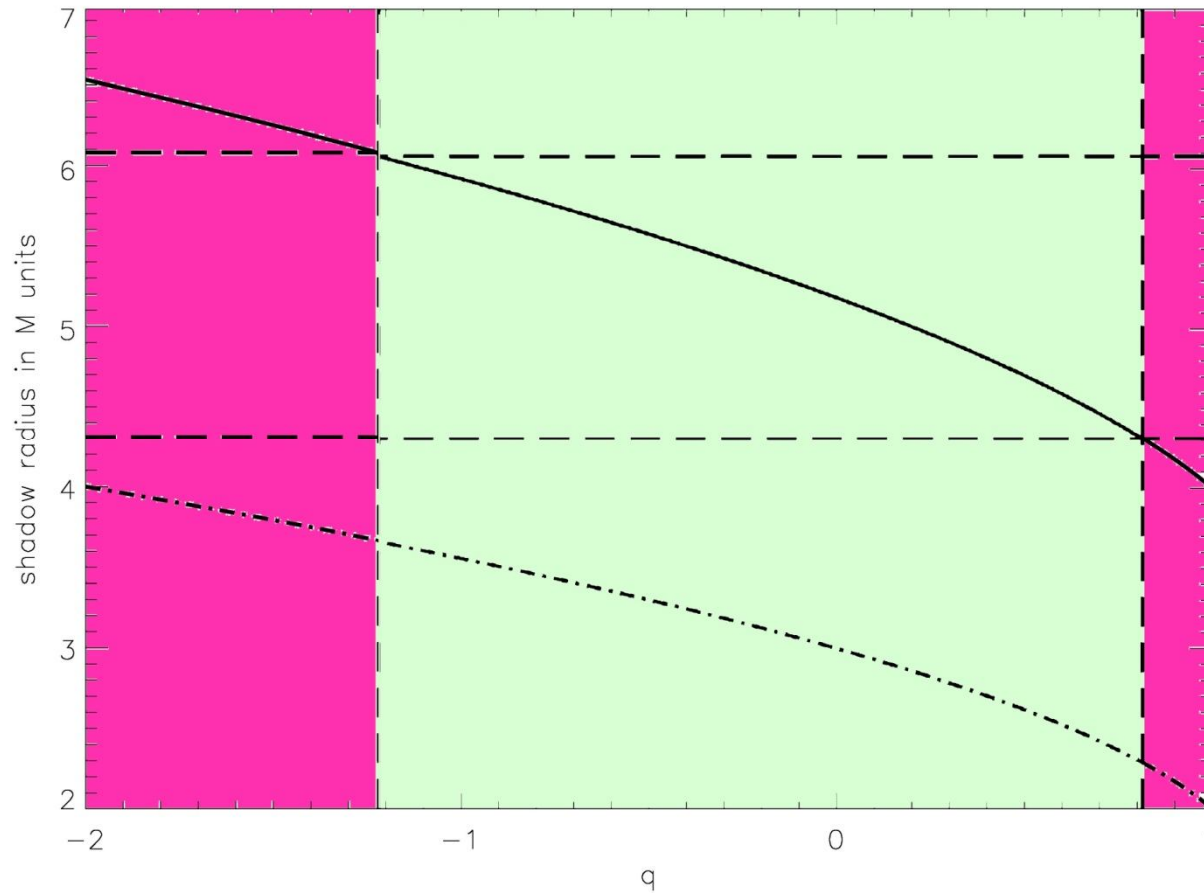


FIG. 3. Constraints set by the 2017 EHT observations on the nonrotating Einstein-Maxwell-dilaton 2 and on the rotating Sen black holes. Also in this case, the gray/red shaded regions refer to the areas that are $1-\sigma$ consistent/inconsistent with the 2017 EHT observations).



Zakharov, Universe, 2022; arxiv:2108.01533; charge constraint
on M87* (for Sgr A* $D=51.8\pm 2.3$ uas, 12.05.2022). For M87
 $D=D_{\text{Sch}}(1\pm 0.17)$



Sgr A* shadow discovery by EHT (reported on May 12, 2022)

Press Conferences around the world (Video Recordings):

Garching, Germany - [European Southern Observatory](#)

Madrid, Spain - [Consejo Superior de Investigaciones Científicas](#)

México D.F., Mexico - [Consejo Nacional de Ciencia y
Tecnología](#)

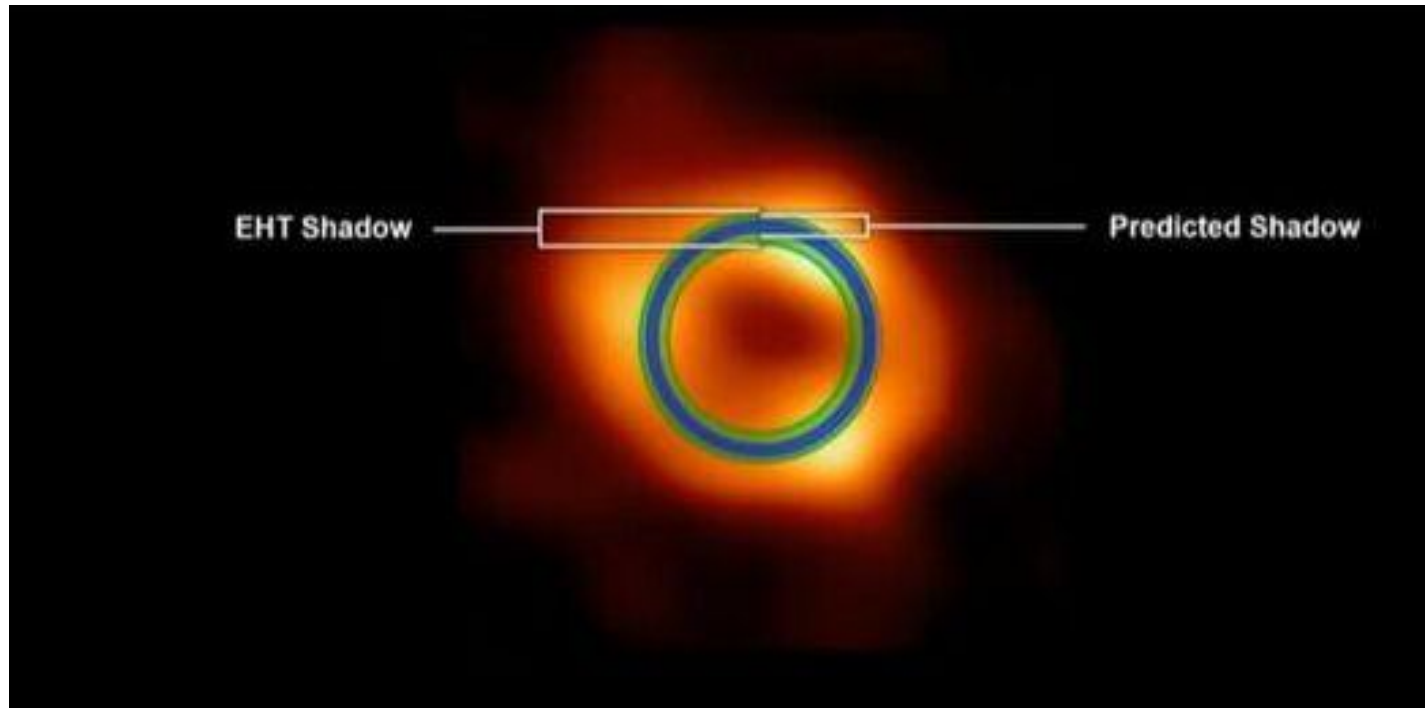
Rome, Italy - [Istituto Nazionale di Astrofisica](#)

Santiago de Chile - [ALMA Observatory](#)

Washington D.C., USA - [National Science Foundation](#)

Tokyo, Japan - [National Astronomical Observatory of Japan](#)

For Sgr A* $D=51.8\pm 2.3$ uas, (EHT collaboration, 12.05.2022)



A. F. Zakharov, Physics of Particle and Nuclei Lett. (2023)

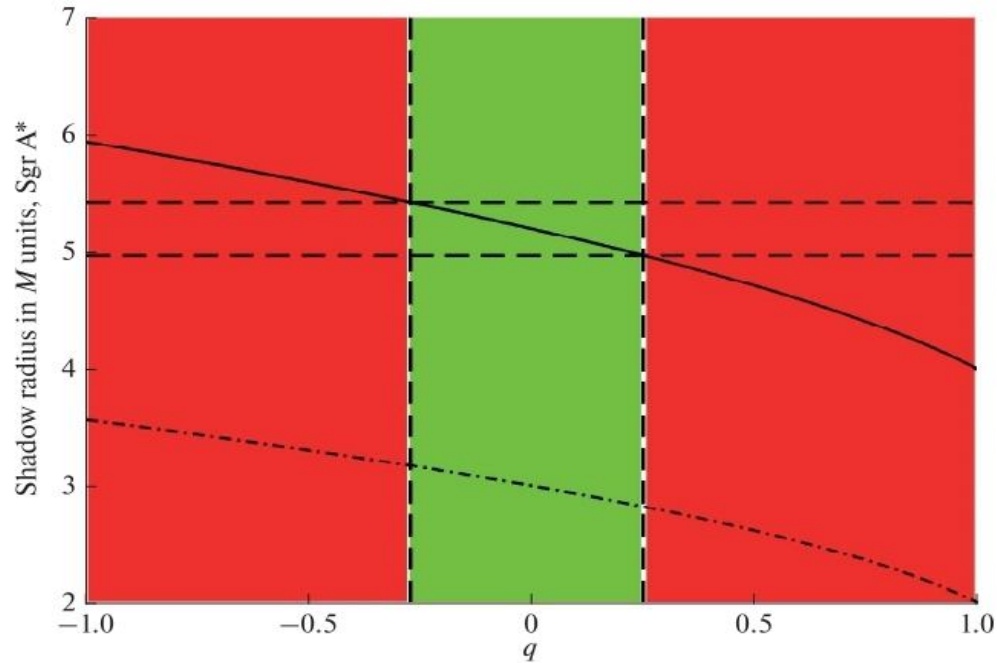
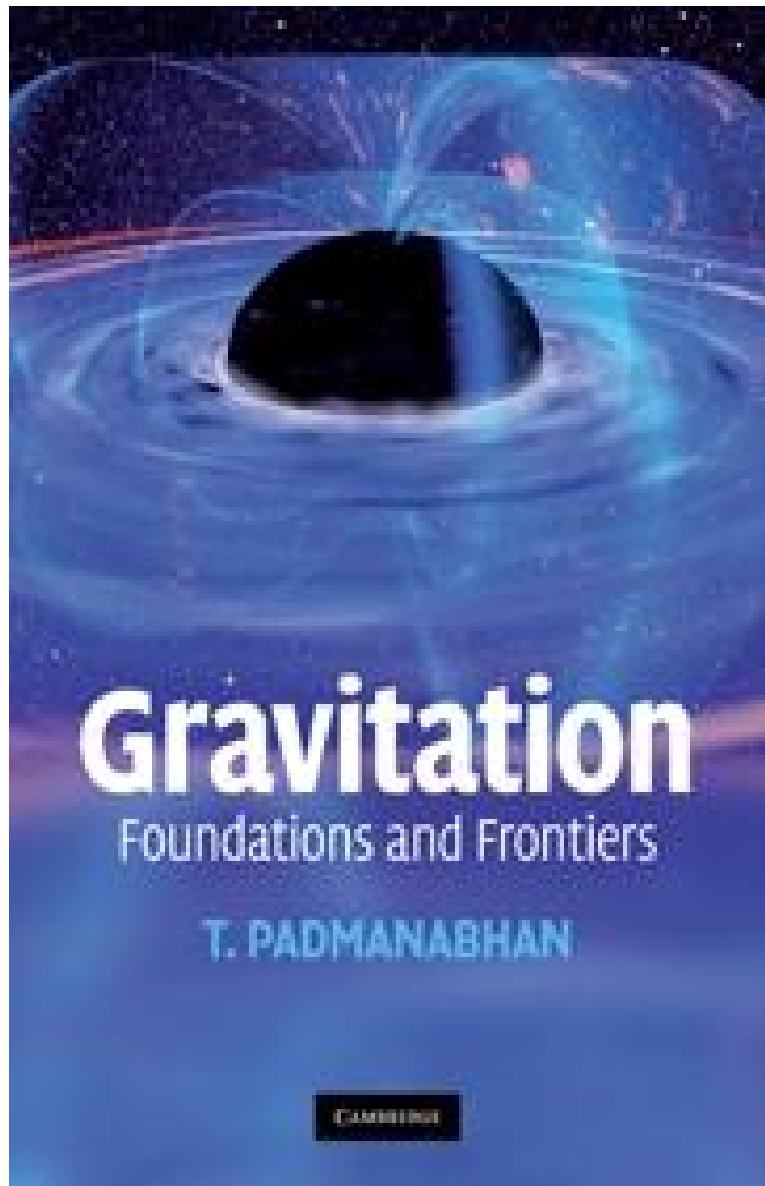


Fig. 1. Shadow radius (solid curve) and radius of the last circular unstable photon orbit (dashed-and-dotted curve) in units M as a function q . Following work [30], we believe that $\theta_{\text{sh SgrA}^*} \approx (51.8 \pm 2.3) \mu\text{as}$ at a confidence level of 68%. The horizontal dashed lines correspond to the restrictions on the size of the radius in units M . Accordingly, red vertical stripes for q are inconsistent with these estimates of the size of the shadow in the HC.





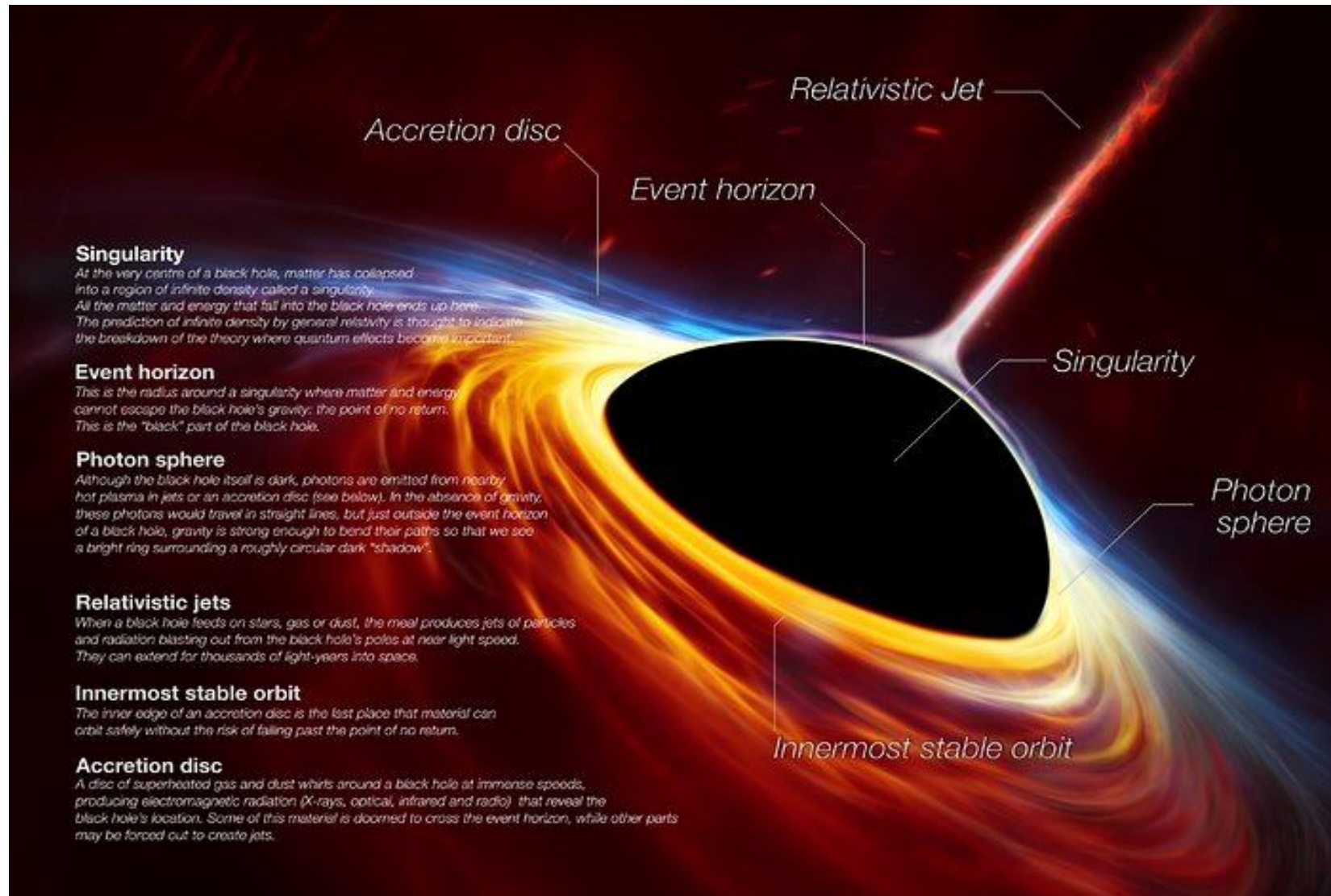
Gravitation

Foundations and Frontiers

T. PADMANABHAN

CAMBRIDGE

The Event Horizon Telescope Picture



Conclusion

The shadow concept has been transformed from a purely theoretical element into an observable quantity which may be reconstructed from astronomical observations.

Therefore, VLBI observations and image reconstructions for M87* and Sgr A* are in remarkable agreement with an existence of supermassive black holes in centers of these galaxies.

- Thanks for your kind attention!



Figure 13. Inset: paint-swatch accretion disk with inner and outer radii $r = 9.26M$ and $r = 18.70M$ before being placed around a black hole. Body: this paint-swatch disk, now in the equatorial plane around a black hole with $a/M = 0.999$, as viewed by a camera at $r_c = 74.1M$ and $\theta_c = 1.511$ (86.56°), ignoring frequency shifts, associated colour and brightness changes, and lens flare. (Figure from *The Science of Interstellar* [40], used by permission of W. W. Norton & Company, Inc. and created by our Double Negative team, TM & © Warner Bros. Entertainment Inc. (s15)). This image may be used under the terms of the Creative Commons Attribution-NonCommercial-NoDerivs 3.0 (CC BY-NC-ND 3.0) license. Any further distribution of these images must maintain attribution to the author(s) and the title of the work, journal citation and DOI. You may not use the images for commercial purposes and if you remix, transform or build upon the images, you may not distribute the modified images.

itself. This entire image comes from light rays emitted by the disk's bottom face: the wide bottom portion of the image, from rays that originate behind the hole, and travel under the hole and back upward to the camera; the narrow top portion, from rays that originate on the disk's front underside and travel under the hole, upward on its back side, over its top, and down to the camera—making one full loop around the hole.

There is a third disk image whose bottom portion is barely visible near the shadow's edge. That third image consists of light emitted from the disk's top face, that travels around the hole once for the visible bottom part of the image, and one and a half times for the unresolved top part of the image.

In the remainder of this section 4 we deal with a moderately realistic accretion disk—but a disk created for *Interstellar* by Double Negative artists rather than created by solving astrophysical equations such as [32]. In appendix A.6 we give some details of how this and other Double Negative accretion disk images were created. This artists' *Interstellar* disk was chosen to be very anemic compared to the disks that astronomers see around black holes and that astrophysicists model—so the humans who travel near it will not get fried by x-rays and gamma-rays. It is physically thin and marginally optically thick and lies in the black hole's equatorial plane. It is not currently accreting onto the black hole, and it has cooled to a position-independent temperature $T = 4500$ K, at which it emits a black-body spectrum.

Figure 14 shows an image of this artists' disk, generated with a gravitational lensing geometry and computational procedure identical to those for our paint-swatch disk, figure 13

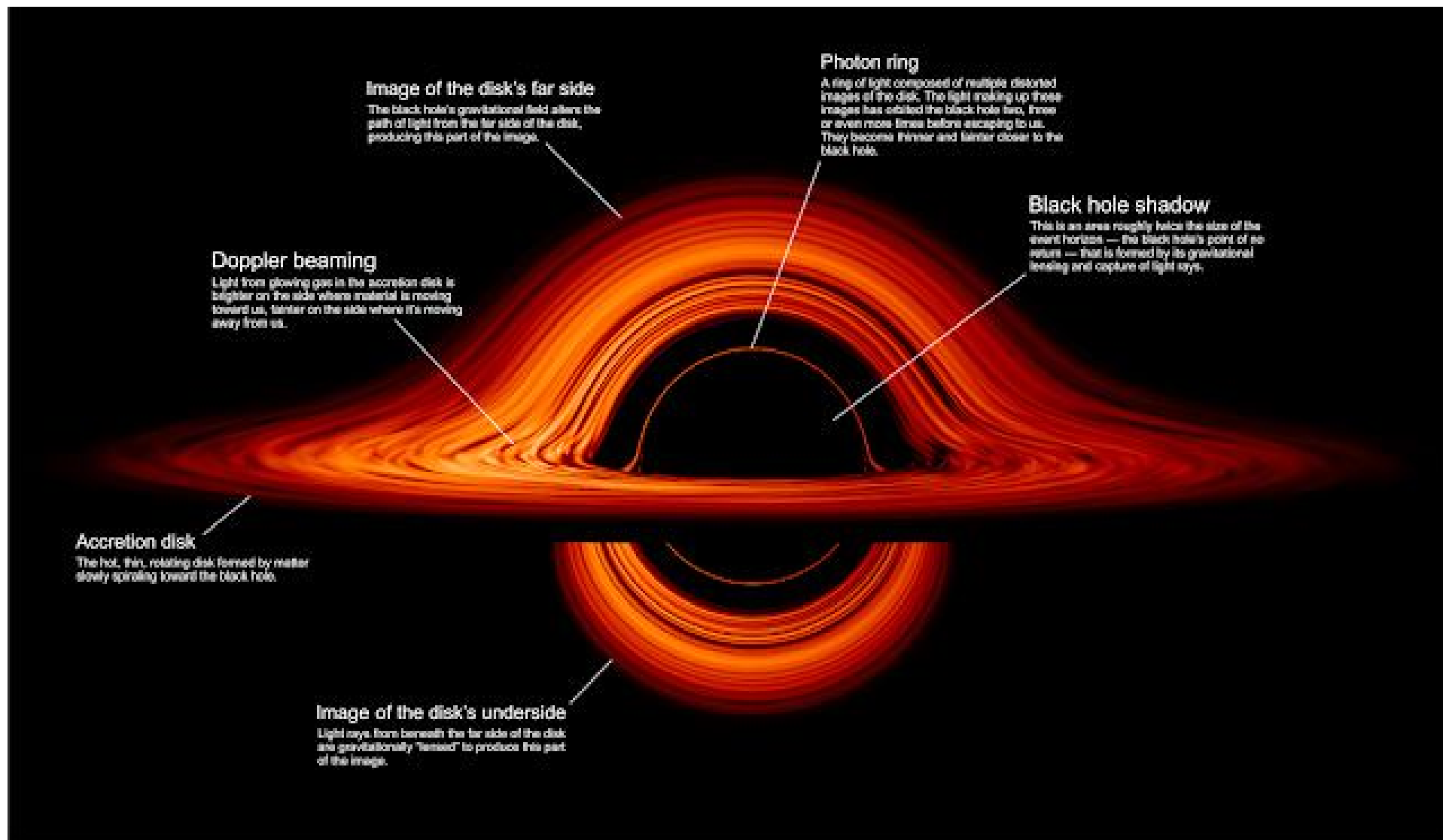


Image of the disk's far side

The black hole's gravitational field alters the path of light from the far side of the disk, producing this part of the image.

Photon ring

A ring of light composed of multiple distorted images of the disk. The light making up these images has orbited the black hole two, three or even more times before escaping to us. They become thinner and fainter closer to the black hole.

Black hole shadow

This is an area roughly twice the size of the event horizon — the black hole's point of no return — that is formed by its gravitational lensing and capture of light rays.

Doppler beaming

Light from glowing gas in the accretion disk is brighter on the side where material is moving toward us, fainter on the side where it's moving away from us.

Accretion disk

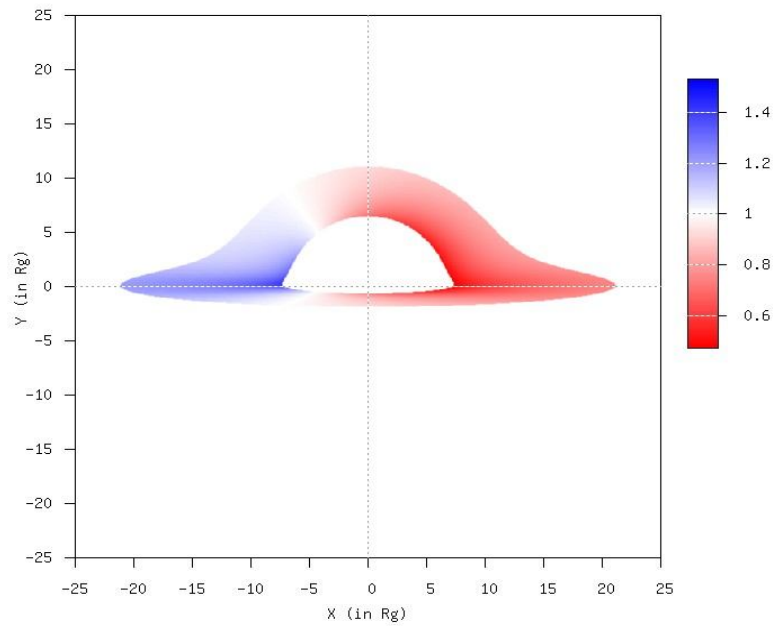
The hot, thin, rotating disk formed by matter slowly spiraling toward the black hole.

Image of the disk's underside

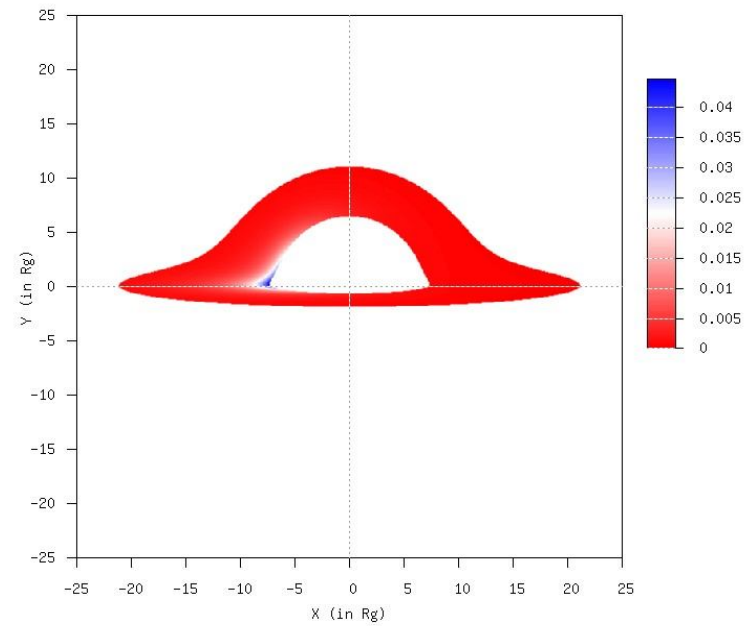
Light rays from beneath the far side of the disk are gravitationally "lensed" to produce this part of the image.

Schwarzschild black hole images: $\theta=85$ deg

- Redshift map

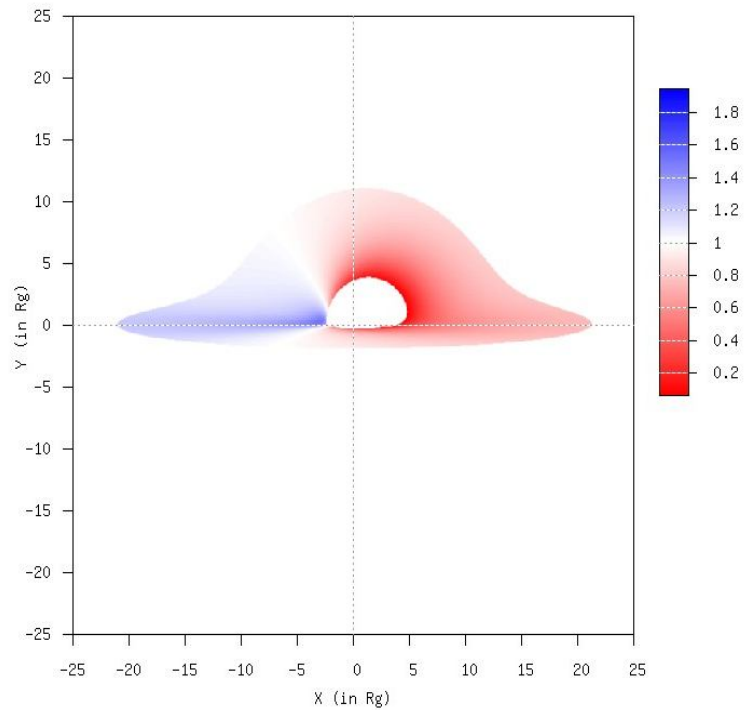


- Intensity map



Kerr black hole images ($a=0.99$): $\theta=85$ deg

- Redshift map



- Intensity map

